The Pennsylvania State University

The Graduate School

College of Engineering

THE DEVELOPMENT OF A SECURITY-SCREENING PORTAL FOR HUMAN AERODYNAMIC WAKE SAMPLING

A Thesis in

Mechanical Engineering

by

Stephen P. Frymire

Submitted in Partial Fulfillment
of the Requirements
for the Degree of

Master of Science

December 2009

The thesis of Stephen P. Frymire was reviewed and approved* by the following:

Gary S. Settles
Distinguished Professor of Mechanical Engineering
Thesis Adviser

John M. Cimbala
Professor of Mechanical Engineering

Karen A. Thole
Professor of Mechanical Engineering
Head of the Department of Mechanical Engineering

*Signatures are on file in the Graduate School.

Abstract

In an effort to increase the throughput of explosive trace sampling in airport security, a trace sampling portal was designed based upon the recirculation region found in the human aerodynamic wake. The human aerodynamic wake has been shown to separate from the body as the human subject turns through an angle while walking briskly. As this wake contains small particles from the skin and clothing of the subject, it can be interrogated and screened for explosive traces. Previous work has been focused on the design of a device to collect and extract these traces for investigation.

The effectiveness and efficiency of the portal system components was the primary focus of this investigation. Characterizing the efficiency of a large-scale particle impactor required the development of several independent experimental and computational approaches to confirm that the impactor was performing to specifications. Laser sheet and wall-tuft flow visualization techniques were employed to diagnose the flow behavior at the impactor inlet, to demonstrate the human wake being carried to the inlet, and to optimize the jet impact timing and location on an average-size human subject.

Through the results of these experiments, the aerodynamic wake sampling portal performance and efficiency have been established and characterized.

Table of Contents

List of Figures

List of Tables

Acknowledgements

I would like to acknowledge the Penn State Gas Dynamics Lab for the opportunity, education and guidance that they have given me. I would like to thank my faculty advisor Gary Settles for all he has taught me about research practices and being a good experimentalist, and that being a good engineer is much more than doing only what is asked of you. Lab technician J.D. Miller and lab manager Lori Dodson-Dreibelbis have helped me through the problems and challenges that arose with all facets of the project. Without them, I would still be stuck at square one.

I would also like to acknowledge my friends and lab mates, Mike Hargather, Matt Biss, Mike Lawson, Tom Liebner, Matt Madalis, and Rory Bigger. They were always there to help me brainstorm, to bounce ideas off of, and to make sure that I lived the good life outside of the lab. And to everyone else who helped me enjoy the life of a grad student, thank you as well.

Without the support, encouragement, and generosity provided by my parents over the last 20 years of my academic career, I would never have been able to get to this level, much less succeed at it the way that I have. I cannot thank them enough.

Finally, I have to thank my girlfriend, Bridget Austin. She did more to get this project completed than I could ever express. Her confidence, encouragement, and patience with the time that it took for me to get to the end were beyond compare. This is as much for her as it is for me.

1.0 Introduction

1.1 – Existing Portal Technology

In an effort to better protect passengers, a number of different techniques has been employed at airport security checkpoints. X-ray machines screen carry-on and checked luggage, metal detectors have long been used to detect weapons and contraband hidden on the passengers themselves, and, more recently, a number of different devices has been introduced to detect explosive and narcotic traces through swabbing luggage or subjects directly or by 'sniffing' to interrogate the human thermal plume. The explosive detection portals recently used in airports require 10-20 seconds per subject, which limits the total number of passengers that can be sampled compared to the total number going through the airport (1).

The test procedure consists of the subject stepping into the portal, the operator firing air jets to dislodge particles from the subject and to help conduct the flow upward, and waiting for the human thermal plume to develop and carry the trace to the overhead sampler with the assistance of a blower (2). This portal design operates on the principle of the human thermal plume, a thermal free-convection layer that develops due to the heat transfer from the warmer human subject to the typically cooler ambient air (Fig. 1.1.)

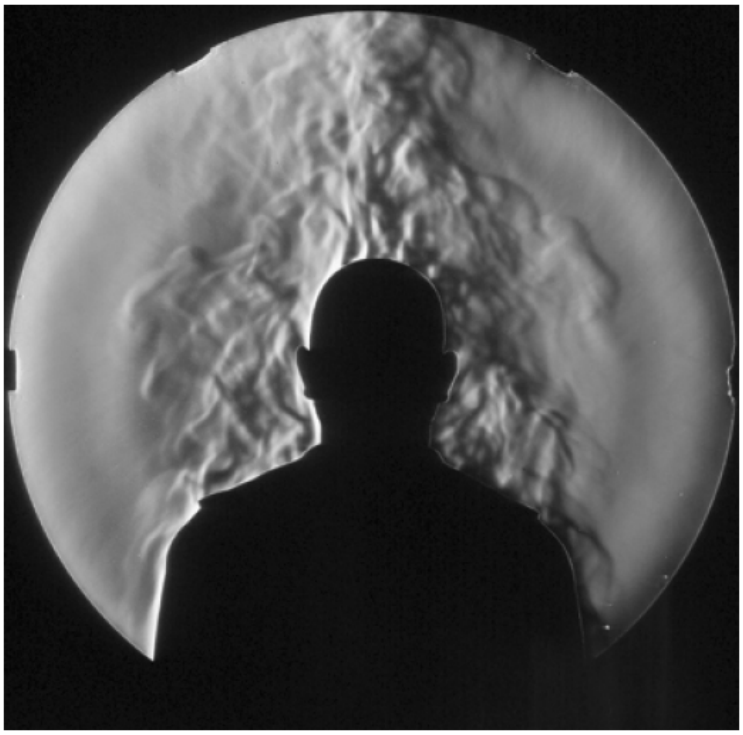

Fig. 1.1 – Human thermal plume visualized using schlieren technique

Experimental and computational studies were conducted to discover that the human thermal plume separates from the body at the shoulders and forms a recirculation region which eventually merges with the flow generated from the top of the head. The buoyant flow has a natural flow rate between 20 and 40 L/s at velocities from 0.1-0.3 m/s (3).

A long-established target sampling time for such portal is approximately 6 seconds per subject. This goal necessitated a very different approach to sampling methodology and portal design. A new, faster throughput method had to be developed in order to increase the number of passengers able to be sampled.

1.2 – Human Aerodynamic Wake Sampling Concept

The current portal technology requires the re-development of the human thermal plume inside the portal after it gets disrupted by the action of entering said portal. The new design bases its collection method on this apparent shortcoming of the flow environment surrounding the human subject. The human body in motion creates a flow geometry similar to that of a bluff body in a crossflow. This imposed crossflow possesses enough momentum to begin dominating the momentum generated by the human thermal plume

at a walking speed of 0.25 m/s, completely overwhelming it by 1.34 m/s as seen in Fig. 1.2 (1).

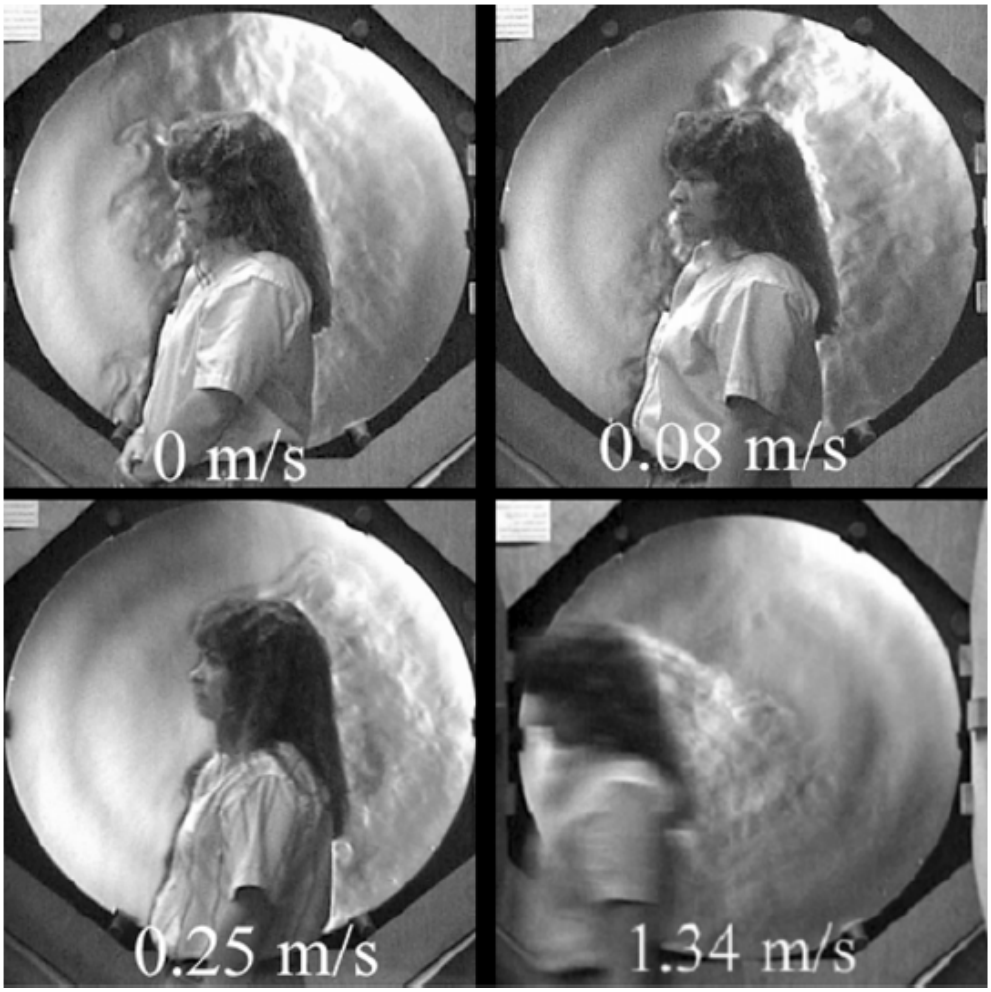

Fig. 1.2 – Thermal plume-to-wake transition visualized with schlieren technique. Images from G S. Settles.

The thermal plume begins to be 'bent over' at the 0.25 m/s mark, when the momentum imparted by the crossflow begins to take over. By 1.34 m/s, the thermal plume no longer possesses notable upward motion, having all of its momentum redirected into a wake-like flow at the rear of the subject. This occurs at a walking speed that could easily be attained by airline passengers moving unburdened through a security checkpoint.

These conclusions were confirmed by Edge (4) in a computational study of the wake behind a walking subject. Additionally, it was shown that there is a large recirculation region immediately behind the human subject that serves to "trap" the thermal plume. This recirculation region collects the particulate matter removed from

the human body and carried upward by the thermal plume, creating a "pocket" of trace signal that moves with the subject (Fig. 1.3).

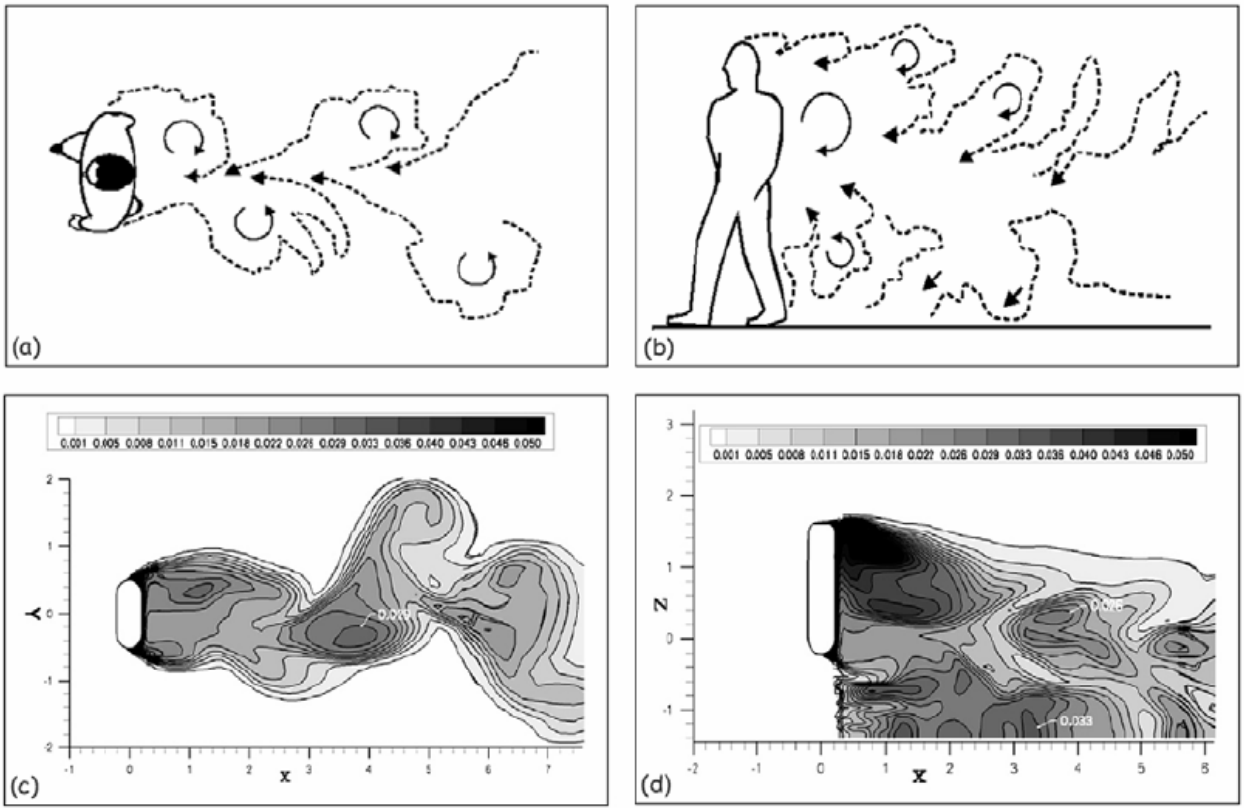

Fig. 1.3 – Comparison of laser sheet flow visualization and CFD model of human aerodynamic wake. (a) Horizontal plane (experiment) (b)Vertical plane (experiment) (c) Horizontal plane (CFD) (d) Vertical plane (CFD). Images from Edge (4).

This figure shows how the flow gets "trapped" behind the human subject. It also shows how the thermal plume gets wrapped around the top and sides of the human subject, virtually eliminating the upward plume flow. Any material released from the body is mixed and spread throughout the wake until a roughly uniform distribution of particulate material is reached in the region between the shoulders and the upper thighs (4).

It was theorized that this human aerodynamic wake, in possession of its own inertia independent of the human subject that generated it, could be separated from the subject moving at a certain walking speed, collected, and interrogated to determine the presence, or lack thereof, of explosive or contraband trace. To confirm this hypothesis, it was necessary to demonstrate that the wake retained its trace material content while moving, and that it could be separated from the human subject. Craven (1) proved both of these to be possible. By seeding the wake with theatrical fog, it was possible to see

that there was significant trace material present even after being carried several meters from the point of fog introduction (Fig. 1.4.)

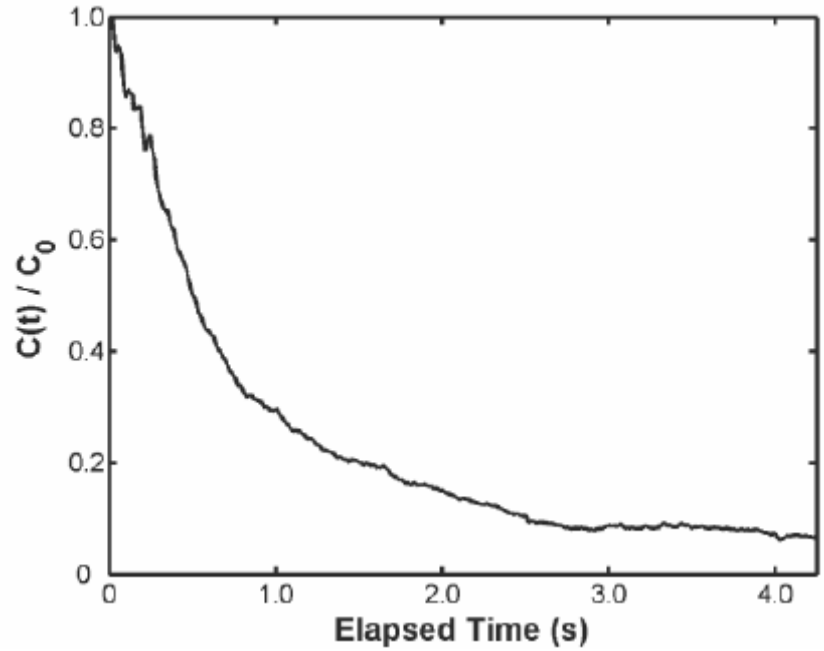

Fig. 1.4 – Decay rate of wake contaminant at a position 3m downstream from wake-seeding location. Image from Craven (1).

This plot shows concentration normalized to the maximum level measured. It does, however, show that there is still a measurable amount of trace material in the wake at 3 m distance, regardless of the quantifiable amount of trace that was initially present. Additionally, it provides the important metric that, after ~3.0 seconds, approximately 90% of the signal present has cleared the sensor (1). This is worth noting in that the fundamental physics that underlie this concept help to approach the throughput goal stated earlier. As the concentration levels drop below 20% after 3-4 seconds, barring any interrogative delays, another human subject could be introduced into the portal for sampling.

The other determination that had to be made for the proof of this concept was the ability to separate the human wake from the subject. A standard phenomenon that results in a flow separation was employed in this experiment. It was assumed that if the subject turned through an angle at speed, the inertia of the wake itself would be unable to undergo such a rapid course change, and would thus separate. Again using a laser sheet

and fog-seeding the human wake, it was possible to visualize the detachment of the wake from the human subject (Fig. 1.5.)

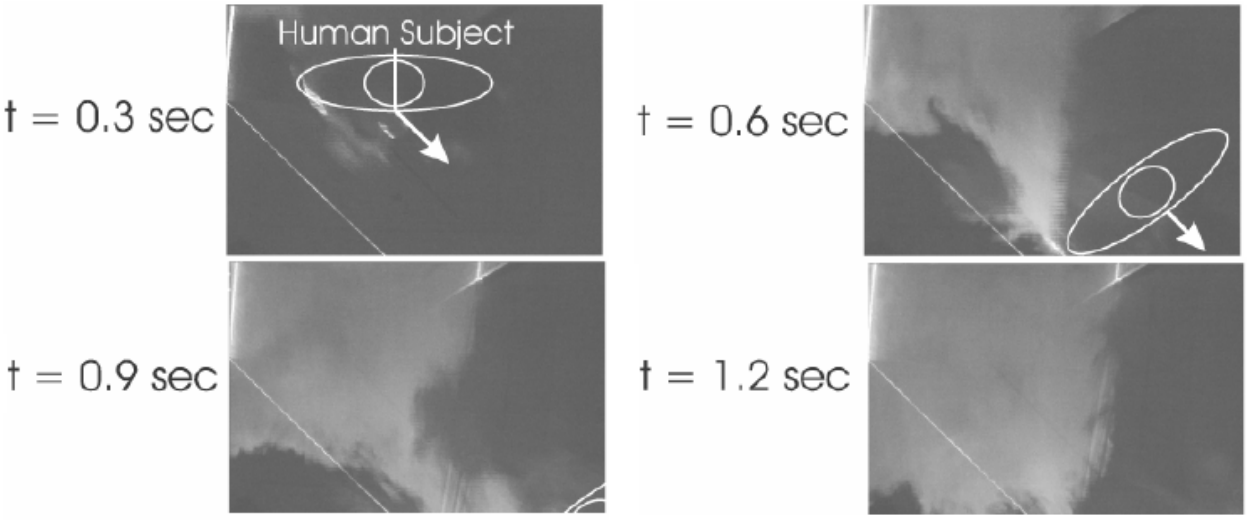

Fig. 1.5 – Top view of wake separation at a 45^{o} turning angle. Images from Craven (1).

The human subject is outlined and its path is indicated by the arrow. The subject enters the top center of the frame at speed and, after 0.9 seconds, exits the bottom right corner of the frame. The wake maintains its initial momentum and stays on the straight top-to-bottom path with which it enters the frame. This shows that the wake can and does separate from the subject and, given the appropriate positioning of interrogation equipment, can be analyzed to determine the presence of explosive and contraband trace (1).

The conclusions drawn by Settles (2), Edge (4), and Craven (1) provide the confirmation of the underlying concepts to this new wake sampling portal design. It has been shown that the trace particulate released from the human body gets transported upwards towards the head and gets trapped in the recirculation region generated by the separation of the walking-induced crossflow around the human body. This contaminated wake is carried along by the human subject, can be separated by the simple act of turning through a 45^{o} angle, and can then be collected for interrogation. Based upon the fundamental physics disclosed, the throughput time of subjects can be as little as ~3.0 seconds.

1.3 - Previous Work on the Aerodynamic Wake Sampling Portal

The aerodynamic wake sampling portal is designed to isolate, capture, and interrogate any trace materials trapped in the complex flow region behind a walking human subject (5). To do this, a new and different approach to portal geometry and function had to be taken. Most notably, the rotation of the entire apparatus to function in the streamwise direction of the walking subject has reoriented and increased the overall footprint of the system, but has reduced the time required to process passengers (Fig. 1.6.)

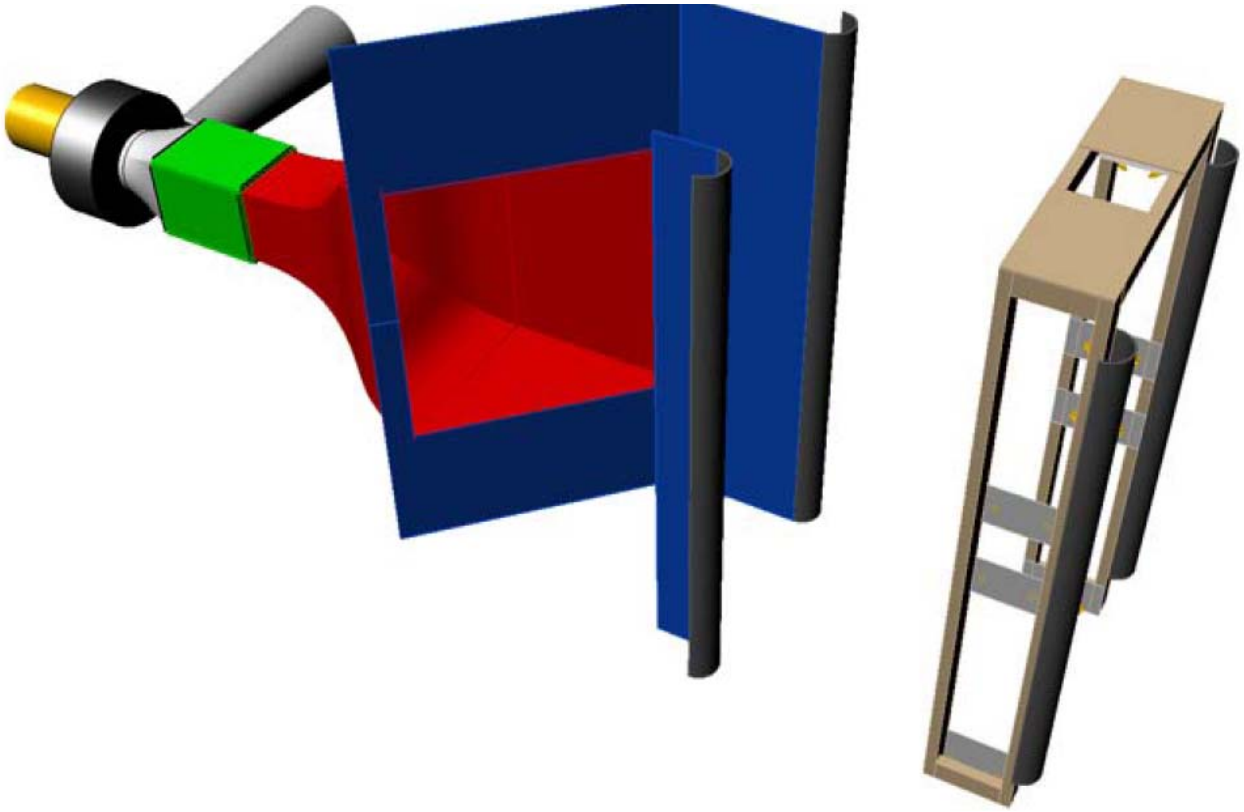

Fig. 1.6 – Perspective view of aerodynamic wake sampling portal concept drawing

Each component had to be taken back to first principles to be optimized for the unique nature of the flow in this case. To better explain the screening procedure, a top view of the portal with functional pathlines is presented below (Fig. 1.7.)

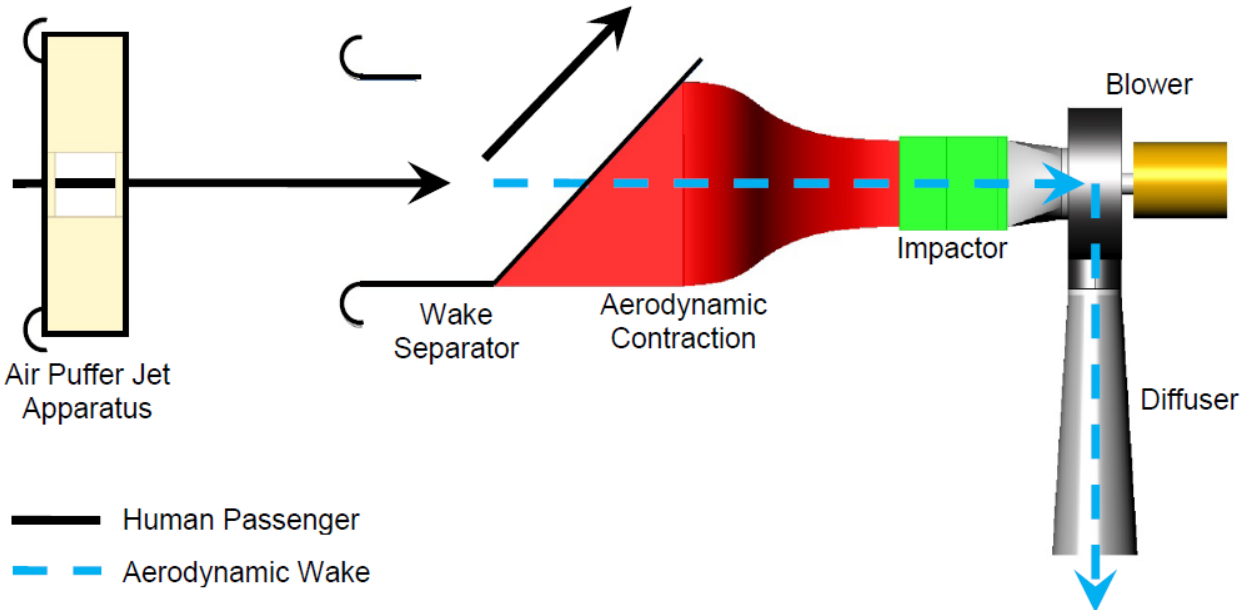

Fig. 1.7 – Top view of aerodynamic wake sampling portal with functional pathlines as indicated

The human subject enters the portal through the air puffer jet apparatus where air jets agitate the clothing, hair, and shoes of the subject to release particles that are entrained in the wake and vectored towards the rest of the portal. Fairings at the edge of the wake separator help to eliminate recirculation regions that could potentially remove and trap trace materials from the human wake. The human subject then makes a 45^{o} sharp left turn, causing the wake to separate due to its independent momentum and enter into the aerodynamic contraction. This contraction serves to channel the flow from a large rectangular inlet to the smaller square inlet of the impactor. With the aid of the blower, the flow is drawn into the impactor where trace particles are extracted from the bulk flow of the wake and concentrated for explosive and contraband analysis. The bulk airflow then exits through a straight-walled conical diffuser which serves to recover some of the energy expended to transport the wake, thus allowing the blower to be operated at a lower power setting (5).

1.3.1 – Air Puffer Jet Apparatus

The air puffer portion of the portal is similar in concept to the air jets used in the current portal designs. The air jets' primary function is to agitate clothing and hair to dislodge any trace materials that may be present. These particles, if light enough, are caught by the momentum of the human thermal plume and brought up into the wake region behind

the torso. However, since the subject is moving through the portal, there is a necessary delay in the triggering of the front versus the rear air puffer jets. The delayed rear jets serve to impact the subject when in the appropriate position as well as help direct the flow of the wake towards the aerodynamic contraction and impactor (5).

1.3.2 – Wake Separator

The wake separator concept was developed and refined by Craven (1). After proving the theory that the human wake could successfully trap and transport a trace signal, studies were conducted to optimize the subject turning angle, the distance between the entrance fairings and the collection orifice plane, and the size and location of the collection orifice. Additional tests were done to measure the effectiveness of this orifice at collecting the wake for sampling.

The optimum turning angle was found to be 45^{o}. From a purely physical standpoint, a sharper 90^{o} turn would be best, however, from a human factor standpoint, this was impractical both due to the severity of the turn and the tendency for most subjects to stop moving in order to make the turn. In stopping, the momentum of the wake carried the bulk of the trace into a collision with the body of the stopped person. This caused re-dispersion into the thermal plume and reduced the amount of the wake that was separated, decreasing the overall effectiveness of the portal design (1).

The size of the collection orifice was chosen based upon human factors guidelines set forth by the DHS Transportation Security Laboratory, the computational results from Edge indicating where the wake was most likely to recirculate and concentrate trace materials based on the average height of a human subject, and Craven's flow visualization experiments regarding the actual location of recirculation regions, the ability of the flow to separate, and the vectoring of the flow by the air jets (4) (1). These points set the rough overall dimensions, which were then further refined based upon the results of the impactor and contraction analyses.

1.3.3 – High Flow Rate Impactor

The most heavily-engineered element of this portal design, as well as its most unique feature, is the impactor. Impactors are defined as devices comprised of a nozzle impinging on a perpendicular plate (Fig. 1.8.)

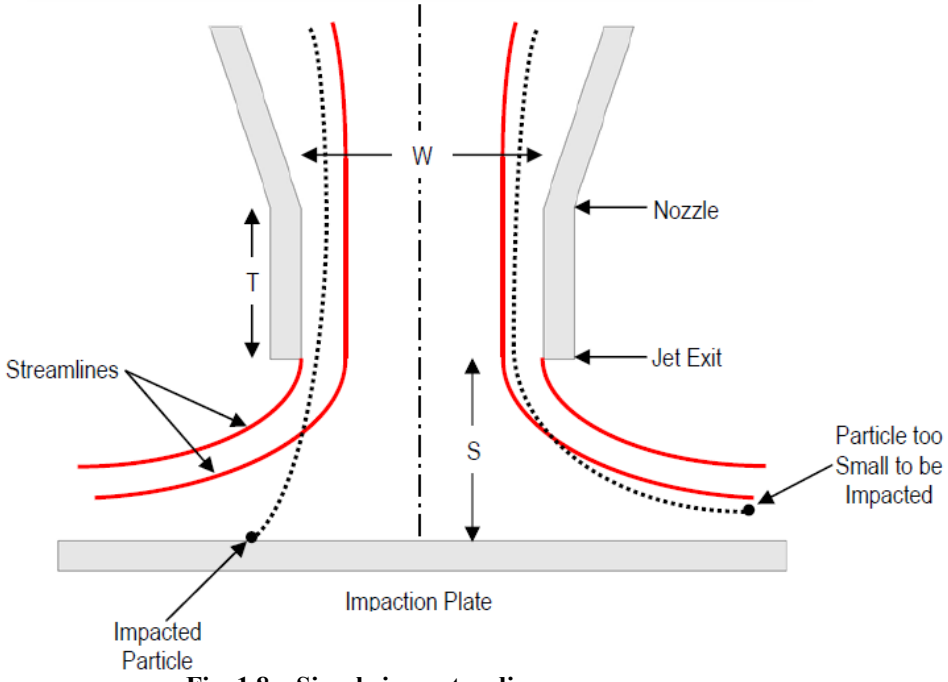

Fig. 1.8 – Simple impactor diagram

Their primary function is to remove particles from an aerosolized flow. Particles with enough mass will be removed from the bulk airflow and, in the wake sampling portal, be concentrated for desorption and sampling. Smaller particles will follow the airflow streamlines and exit the impactor completely. This fundamental impactor design was the starting point for the optimized design of the large-scale high flow rate impactor conducted by Volpe (5).

An extensive list of assumptions and requirements, dictated by both geometric constraints on portal system components and desired flow characteristics, was generated to define the impactor design space. Multi-dimensional analysis was used as a first step towards optimizing the basic impactor geometry following multiple iterations to refine the range of the design space. Following the optimization process, a first-attempt model was generated and the flow was simulated using a Navier-Stokes CFD code called FLUENT 6.3 (Fig. 1.9.)

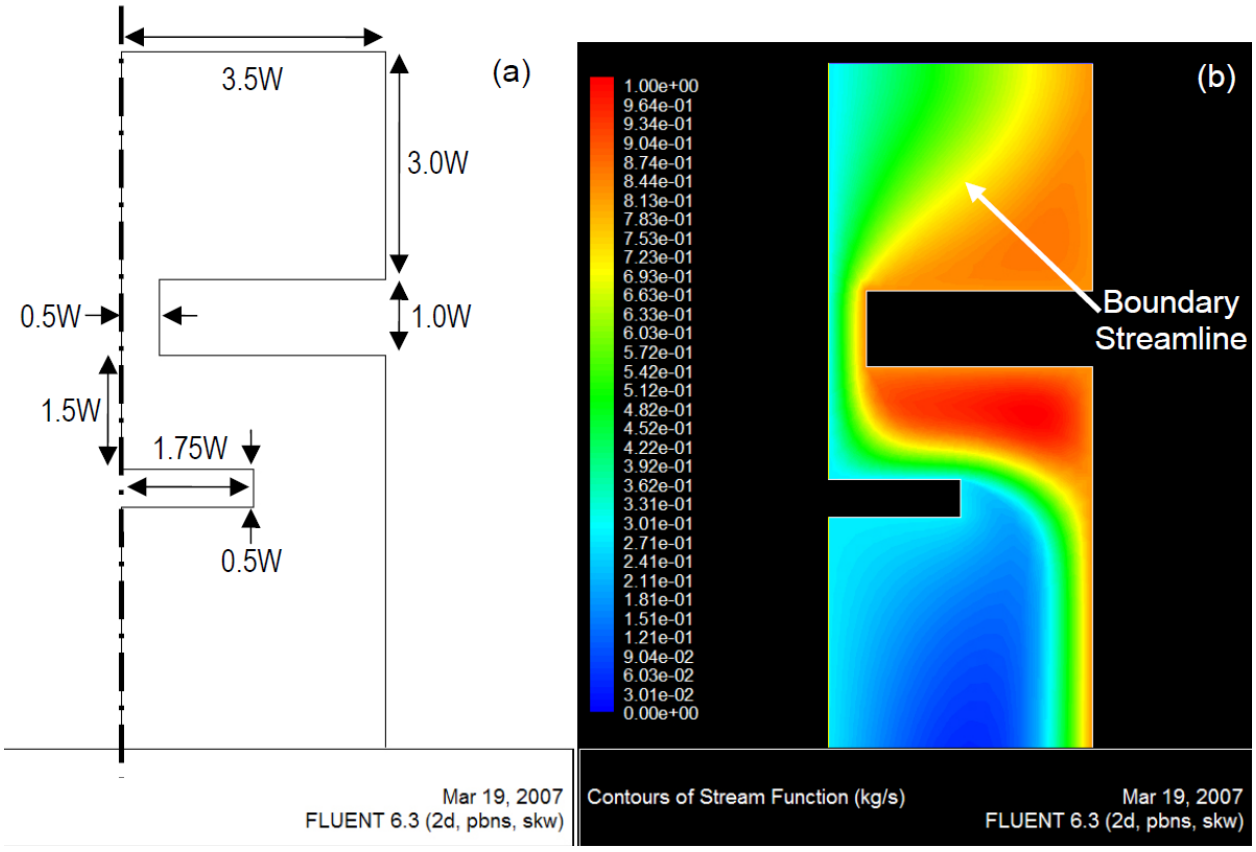

Fig. 1.9 – Fundamental impactor geometry used to generate final design. Flow is from top to bottom. (a) Geometry and dimensions (b) Plot of stream functions of the flow. Images from Volpe (5).

This model was refined based upon streamlines to eliminate separation regions, produce a more uniform flow at the nozzle inlet, and reduce the overall pressure loss through the impactor, thereby reducing the amount of power required to move the contaminated wake through the portal. The "boundary streamline" was chosen and, with some further curve smoothing and geometric adjustments, the final two dimensional parameters were set (5).

Based upon the geometry generated from this detailed analysis, the full three-dimensional impactor could be designed. However, to achieve the desired flow parameters, the length of the impactor was such that the practicality of the design came into question. By forcing some of the physical dimensions and changing the impactor from a one-slit to a three-slit design, the impactor geometry achieved a manageable size that retained the desired complex flow characteristics (Fig. 1.10.)

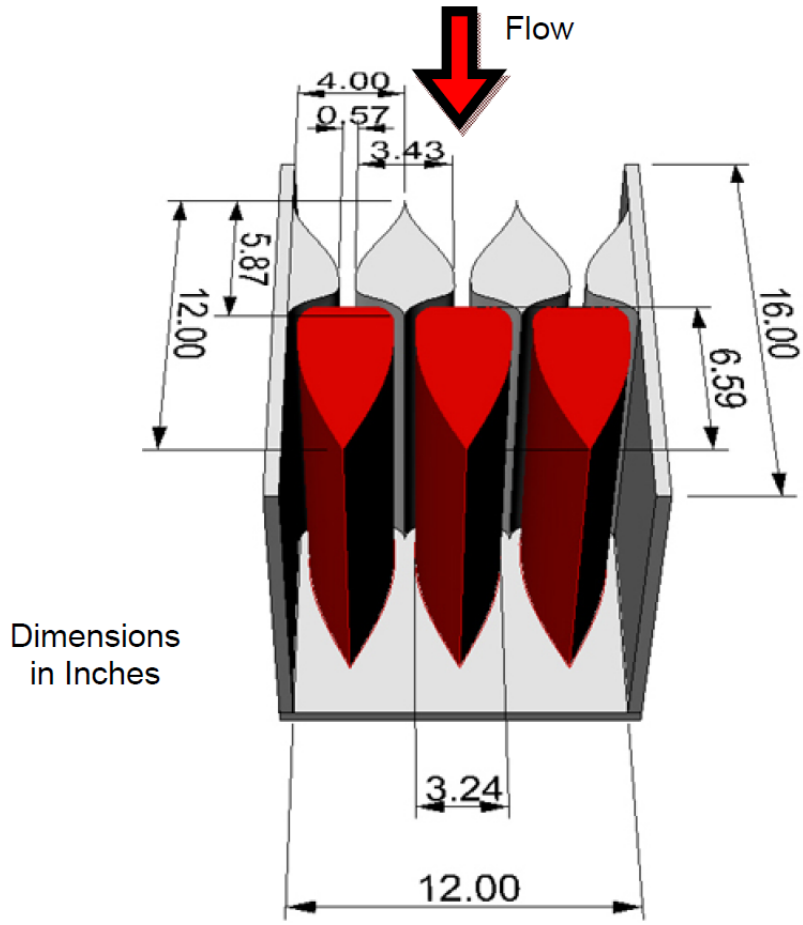

Fig. 1.10 – Final impactor design with side walls removed to show detail of 3-slit design. Image from Volpe (5).

This design allowed the target particle sizes to be captured, the impactor to interface well with the rest of the portal system, and the power requirements to fit within the desired range. The optimization of the impactor also forced an increase of the size of the collection orifice, allowing more of the available wake to be sampled by the portal (5).

1.3.4 – Aerodynamic contraction

The primary function of the aerodynamic contraction is to transport the collected wake from inlet the orifice to the impactor via a smooth low-loss transition. Additionally, the contraction serves to reduce the scale of the flow from the large ~1.0 m^2 inlet size to the ~0.093 m^2 (1.0 ft^2) impactor size. Design principles were taken from the design of subsonic wind tunnels to govern the generation of the contraction wall geometry. There were a number of important design factors considered: the contraction length to minimize the overall system footprint, the location of the match point which determines the

location of the inflection point along the wall, which, in turn, determines whether the flow conditioning favors the inlet or the outlet, and the power factor which affects the steepness of the wall curves, enhancing the exit flow uniformity and minimizing pressure gradients and crossflow generation (5). Following the optimization of these design variables, a computational model was used to simulate the flow behavior through the contraction. This model indicated that the chosen design introduced minimal pressure losses and provided uniform flow conditions at the contraction outlet/impactor inlet, which was an important requirement for the effective collection and analysis of trace signal from the human aerodynamic wake.

1.4 – Current Project Goals

As there has been extensive engineering already conducted on the design of the important components of the wake sampling portal, the primary goal of this thesis is to evaluate the performance of these components when combined in a 'breadboard' portal. The components were fabricated and the portal was assembled to the specifications generated by Craven (1) and Volpe (5). There are three important aspects to the successful implementation of this portal geometry to be evaluated in this thesis: trace particle removal, wake transport, and trace collection by the impactor.

- **Particle Removal**: Develop a better method to trigger the jets, accounting for variability in human size and speed. Demonstrate that the improved jet timing and aiming scheme achieves full coverage of an average human subject.
- **Wake Transport**: Use laser sheet flow visualization to show that the human aerodynamic wake possesses the ability to entrain particles, that these particles get collected in the wake of a walking subject, and that the wake sampling portal is effective in separating and collecting the wake of a human subject as they progress through the portal.
- **Trace collection**: Characterize the impactor efficiency and determine the 50% cutoff particle size diameter experimentally to confirm that the impactor is performing to its designed specifications.

2.0 – Impactor Efficiency Study

Understanding the efficiency of the impactor in this explosive trace sampling portal is critical to determining the overall system performance. Previous work on impactors has been conducted on a smaller scale that enabled researchers to analyze particles in ways that are unfeasible for the wake sampling portal, given its unique flow parameters and size. New approaches had to be employed here to demonstrate the collection efficiency of the impactor.

2.1 – Existing Impactor Efficiency Experiments and Results

There are different methods used by researchers to measure impactor efficiency. The procedures typically begin with a controlled release of mono-disperse particles. These particles are then collected on the impactor face and counted using a method based upon the type of particle. Solid particles can be collected on glass plates or filters for counting via microscopy, or massed on quartz crystals by measuring the change in the crystal's natural frequency. Metallic particles can be charged at the inlet and the change in current across the impactor faceplate can be measured as the particles are collected (6). Fluorescent aqueous particles can also be used to characterize an impactor. They are collected, evaporated, and the level of fluorescence measured before and after impact to quantify the efficiency (7).

In order to compare these different methods, used for different impactor types and geometries, there needs to be a standard representation of impactor efficiency. The standard method of presentation is collection efficiency: the ratio of particles collected to particles released, versus particle size, presented either in terms of diameter or Stokes number. The standard comparison point is called D50, or the diameter at which 50% of the particles released are collected. These curves can also be used to present the results from computational studies, providing a theoretical reference point to validate experimental data (Fig 2.1.) .

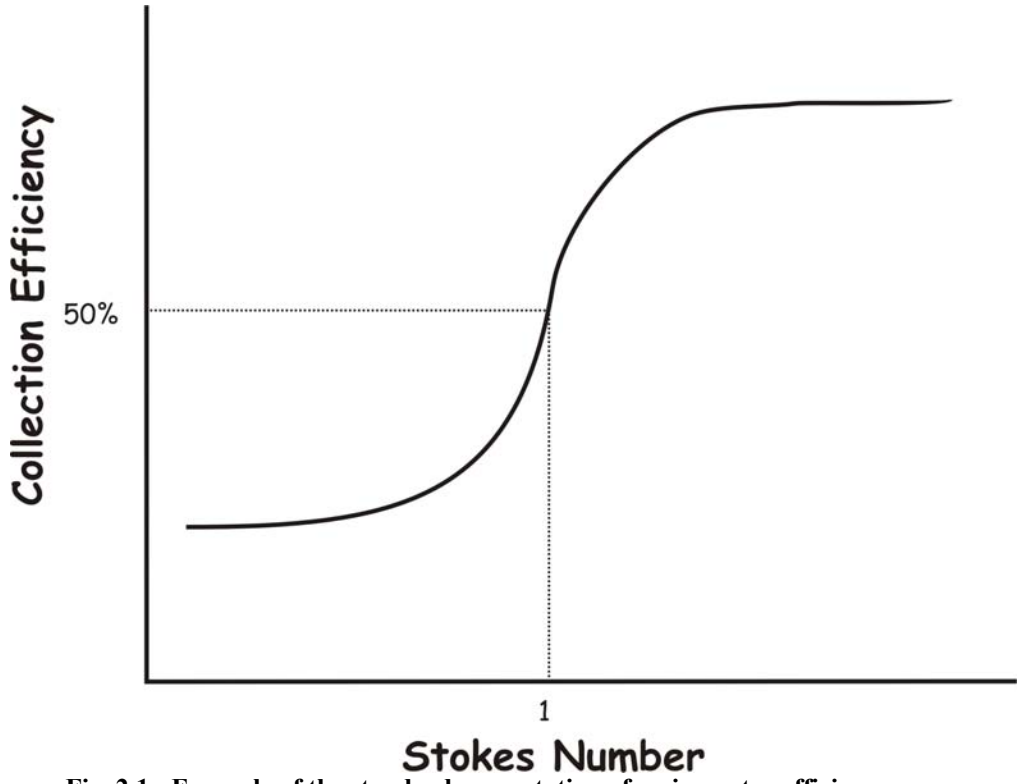

Fig. 2.1 - Example of the standard presentation of an impactor efficiency curve

These existing methods could not be used for this system due to size, flow rate, and overall system geometry. The particles impacted in the wake sampling portal are not able to be introduced in this same manner during normal operation. Particles of a wide size range will be liberated from the subject moving through the portal, meaning an uneven introduction of polydisperse particles will have to travel through the air and be collected by and transported through the contraction before being impacted on a plate. The impactor plate being studied is orders of magnitude larger than what has been used in earlier experiments of this nature. Therefore, controlled release of pre-counted particle doses is impractical, prohibitively expensive, and not representative of how the impactor will be used to screen subjects. Thus, a new method for large-scale impactor characterization had to be developed.

2.2 – Simulant for Contaminated Wake

Since there was not currently a feasible or economic method for introducing monodispersed, counted test particles into this impactor geometry, a different approach had to be taken. In the initial design phases, the densities of several common explosives

were analyzed and an average value, 1.6 g/cc, was assumed to act as the representative density for further design considerations (5). This was used to determine the Stokes number of the particles, a non-dimensional parameter that measures the particle stopping distance relative to the half-width of the impactor.

$$Stk = \frac{\rho_P Q D^2}{9 \mu L W^2} \qquad \textbf{Eqn. 2.1}$$

Where ρ_P is the particle density, Q the bulk fluid volumetric flow rate, D is aerodynamic cutoff/minimum impacted particle diameter, μ is the viscosity of the bulk fluid, L is length of rectangular jet, and W represents width of rectangular jet at nozzle exit. A standard impactor design condition is a Stk = 1.0, meaning that every particle subject to the same flow conditions and geometry whose diameter results in a Stokes number greater than 1.0 should be impacted (8). This was the design point used to generate the final design conditions of the impactor for the wake-sampling portal (5).

With the impactor design set to collect particles larger than Stk = 1.0, it was possible to generate a large-volume particle-laden flow to be used for tests. As the Stokes number is a non-dimensional representation of particle behavior, a different substance, with a known density and size, can accurately simulate the aerodynamic behavior of the explosive trace particles. Talc powder, with a measured density of ρ_P = 2.8 g/cc, was used due to its abundance, safety, low cost, and wide range of particle sizes (Fig. 2.2.) In matching the flow parameters of the design, Stk = 1.0, it was determined that talc particles with a diameter larger than ~4.0 μm should be collected with near 100% efficiency. This range of particle sizes provides the best case in terms of explosive trace detection as the target for improvement in particle detection is particles with a diameter greater than 10 μm, which this impactor is designed to capture (9).

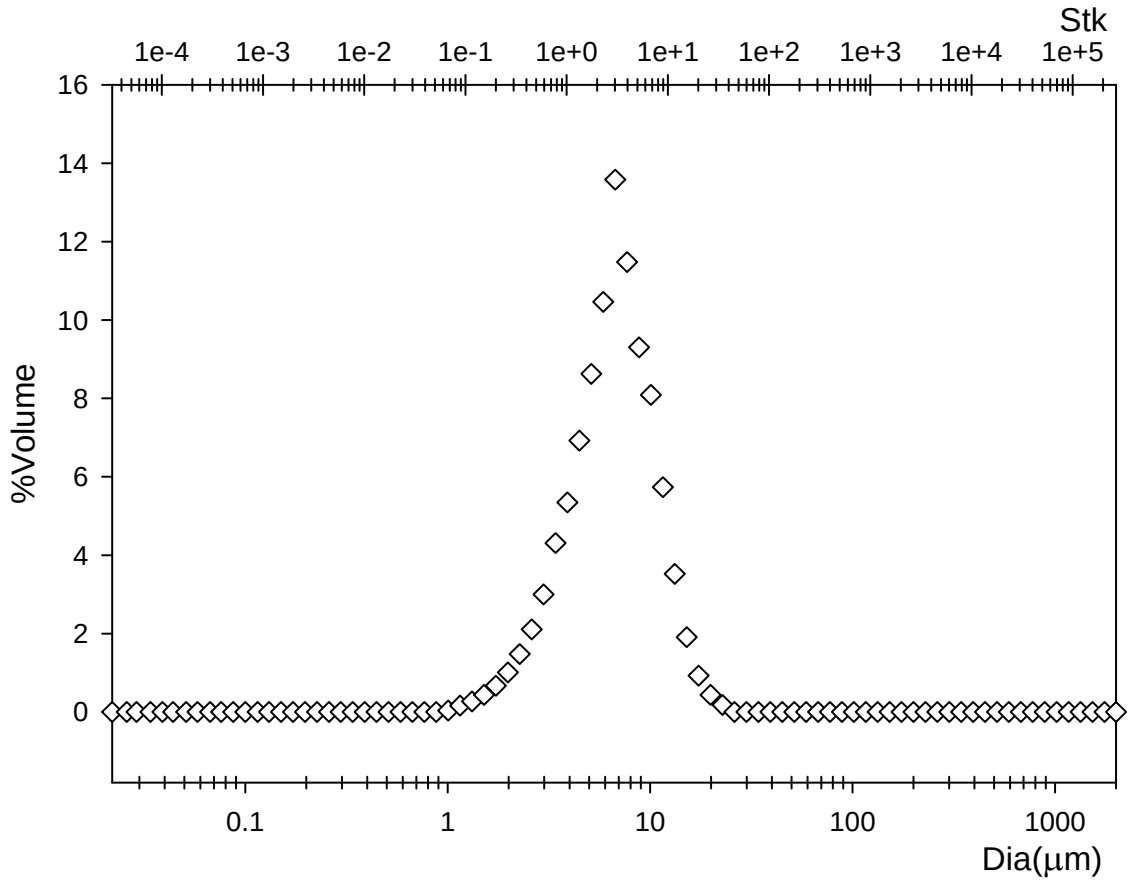

Fig. 2.2 – Standard size distribution of talc in percent volume as a function of diameter

The large flow volume and velocity of the wake-sampling portal required a large, repeatable flow of non-agglomerated particles in order to accurately simulate the transport of trace from the subject wake to the impactor. A fluidizing bed, consisting of plastic beads encased in a length of PVC pipe, was used to break up larger agglomerations and provide a more uniform particle size distribution. Talc powder was loaded into the bottom of the bed and 100 psi shop air was applied for 5 seconds to agitate the powder and beads. A length of 1" diameter tubing directed this stream of particles into the flow of air to be sampled by the impactor (Fig. 2.3.) To avoid the particle stream being directly deposited on the impactor plates, the fluidizing bed was placed such that the stream began at the point where the jets would impact the human subject and dislodge any particulate contained on their person.

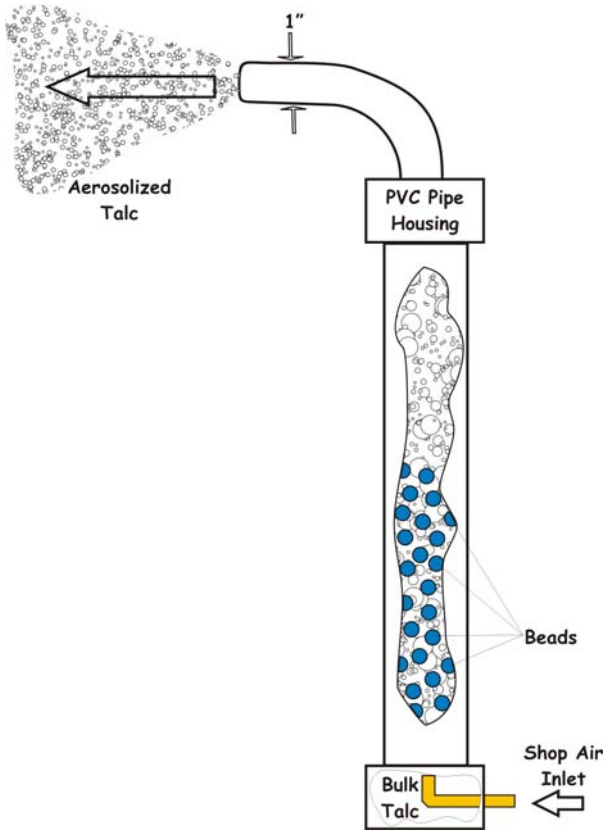

Fig. 2.3 - Diagram of fluidizing bed, including cutaways to show internal function

To estimate the flow rate of particles into the bulk airflow, the simple, incompressible, steady Bernoulli equation was used (Eqn.2.2.)

$$P_1 + \rho\frac{V_1^2}{2} + gz_1 = P_2 + \rho\frac{V_2^2}{2} + gz_2 \qquad \textbf{Eqn. 2.2}$$

State 1 was taken at the shop air inlet, with P_1 being the gauge pressure, V_1 being the fluid velocity, and z_1 being the flow height at that point. State 2 was taken at the outlet of the 1" tube on the top of the fluidizing bed, with the same nomenclature applied to the variables. To simplify the equation, the following assumptions were used: the velocity at state 1 and the gauge pressure at state 2 were assumed to be zero, the change in height was assumed to be negligible, the density was treated as a constant. This yielded an outlet volumetric flow rate though the 1" tube of $0.0176 m^3/s$, run for 5 seconds for each experiment.

This experimental setup allowed a variety of repeatable tests to be conducted to characterize the performance of the impactor. Collection tests were done to determine the size distribution of particles collected on the impactor plates. Total size distributions

within the bulk airflow were also analyzed to determine what range of particle sizes was removed by the impactor.

2.3 – Collection Experiments

The best evidence of particle collection comes from directly analyzing the deposits found on the face of the impactor plates. When using the fluidizing bed and talc powder, it is possible to observe the extraction of particles from the flow by the naked eye (Fig. 2.4.)

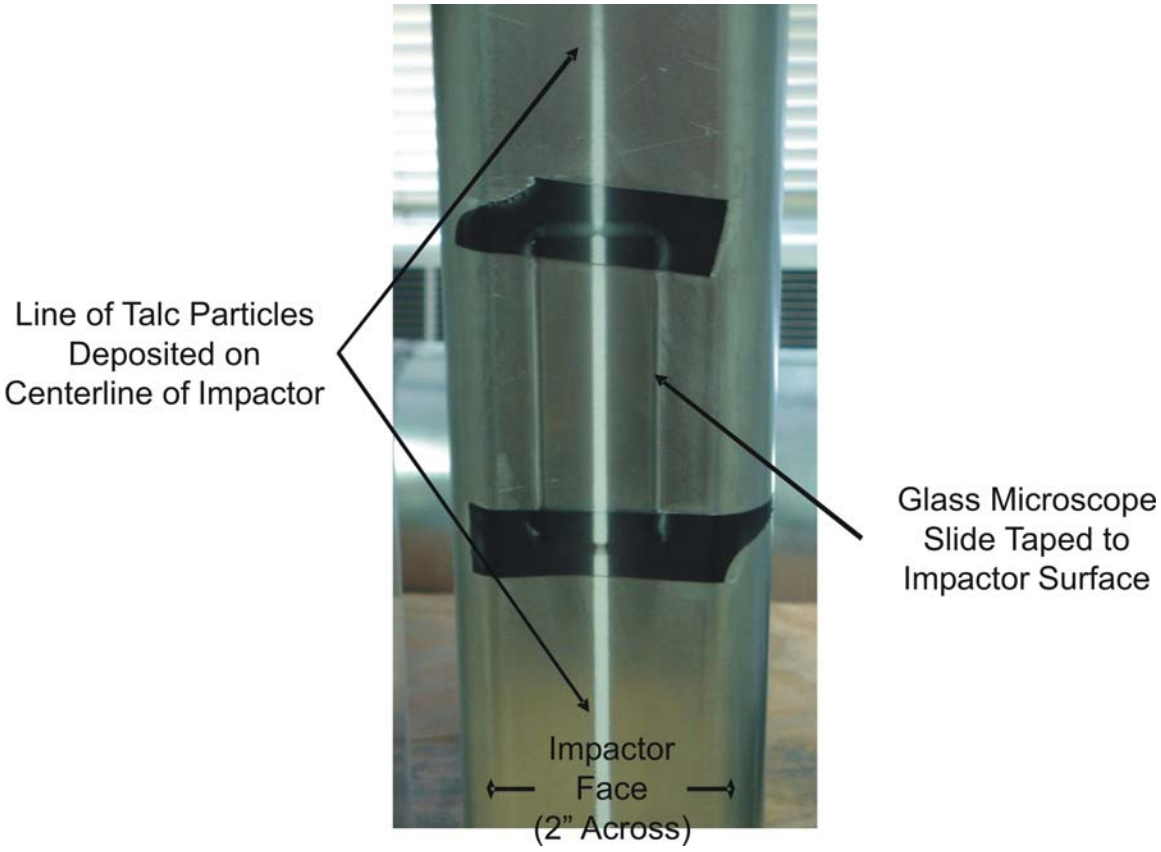

Fig. 2.4 - Visual evidence of talc collection on impactor face

There is a clear concentration of particles along the impactor plate centerline that tapers off towards the lateral edges. To better understand what is going on in terms of actual particle collection, glass slides were attached to the face of the impactor plate. These slides were then analyzed with a microscope to size and count the particles collected on them. Before a thorough analysis of the collected sample could be conducted, however, it was first necessary to demonstrate that there was no flow predisposition to one plate or another or from top to bottom across the plates themselves.

2.3.1 – Collection Analysis Procedure

To collect the particulate media, microscope slides were attached along the impactor plate centerline using electrical tape (Fig. 2.4.) These slides were placed under 10x microscope magnification and images were collected. For the studies determining the flow behavior top to bottom, images were taken horizontally across the plate. This practice served two purposes: 1) enabling the size distributions from side to side to be compared across the vertical range of each impactor plate individually, and 2) enabling the evaluation from plate-to-plate by comparing relative distributions at the same position. These images were processed by a MATLAB code that first converted them to black and white, then counted the particles based upon size (Fig. 2.5.) The counts are presented as a function of position and size, allowing for direction comparison from distribution to another.

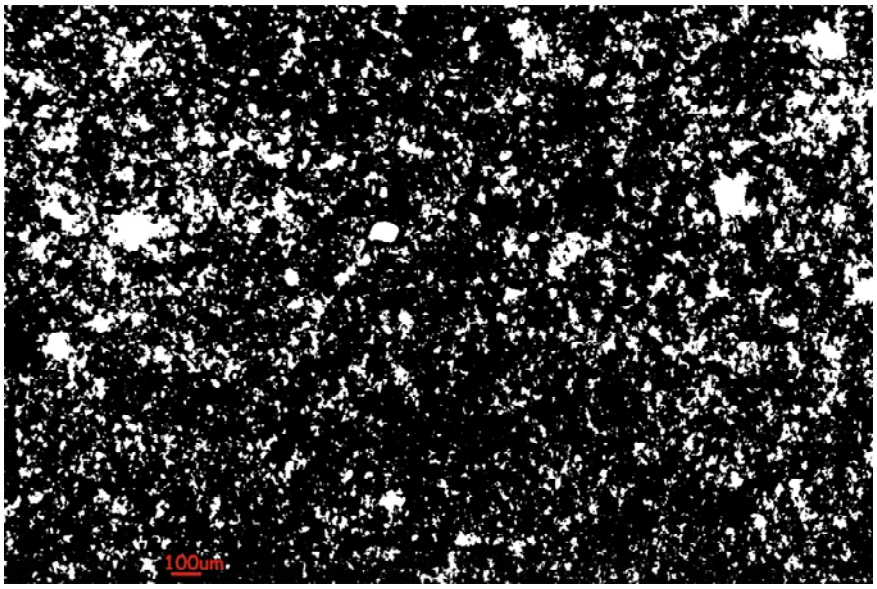

Fig. 2.5 - Magnified (10x) image of particles (white) collected on slide attached to impactor plate

Figure 2.5 shows a typical magnified image of collected particles. It is clear that there is a large range in particle sizes, along with some agglomeration. It is a possible source of error in tests using this aerosolized flow is particle agglomeration. Agglomerations could skew the results to misrepresent the counts and size distributions. It was necessary to conduct an additional experiment to determine what effects the agglomeration has on the particle collection results.

The two possibilities are that the particles agglomerate on the surface as multiple particles impact in the same location and in the bulk fluid flow and impact as a single, larger particle. The former presents a significant source of error as it affects the particle distribution that is collection from the airstream. The latter does not reflect particle collection error. If the particles agglomerate in the airstream, they behave as a single larger particle, which would be expected to behave as if it were large from the initial introduction into the impactor. The standard size distribution of talc particles was used to set the upper and lower bounds of the microscopy analysis. Any particles above the size of the largest particles measured in the talc were classified as agglomerations.

An experiment using a very sparse particle stream was conducted to determine the dominant mechanism of particle agglomeration. A representative image of the typical impact of a large, >30 μm, particle is shown below in Figure 2.6.

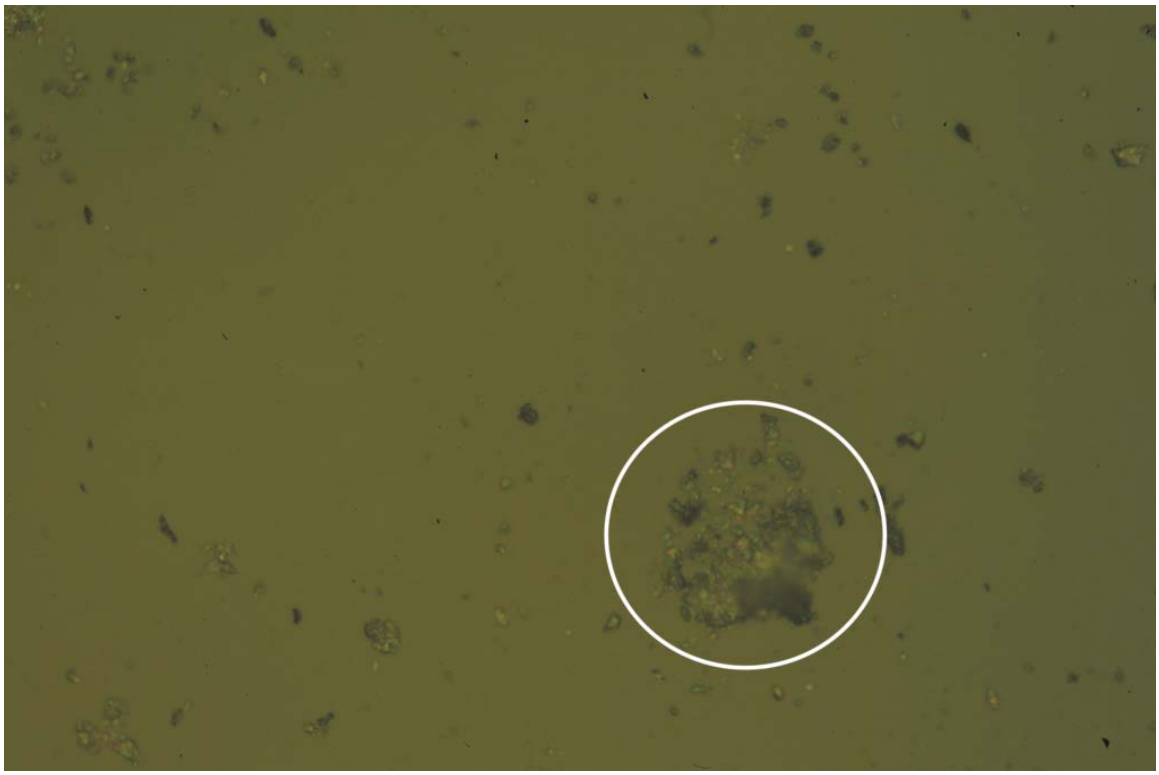

Fig. 2.6 - Representative image of typical impacted large particle.

The large particle in the lower left quadrant of the image is clearly a very large, ~75 μm, particle known to be an agglomeration based upon the particle sizes measured in the aerosolized flow. It impacts on the surface of the slide and partially breaks apart, as evidenced by the array of smaller particles around the larger one. By seeing the impact in

this sparse case, it is clear that the majority of the agglomerations are occurring in the airstream, not on the impactor faces.

2.3.2 – Variation of Collected Distribution: Top to Bottom on an Impactor Plate

The other variable potentially affected by flow behavior is the variation of signal collection in the vertical span of the impactor plates. To measure this, microscope slides were attached to cover the entire height of the plate and images were taken at positions every half inch from top to bottom. The particles were then counted and the distributions were plotted as a function of non-dimensional particle diameter and vertical position (Fig. 2.7.)

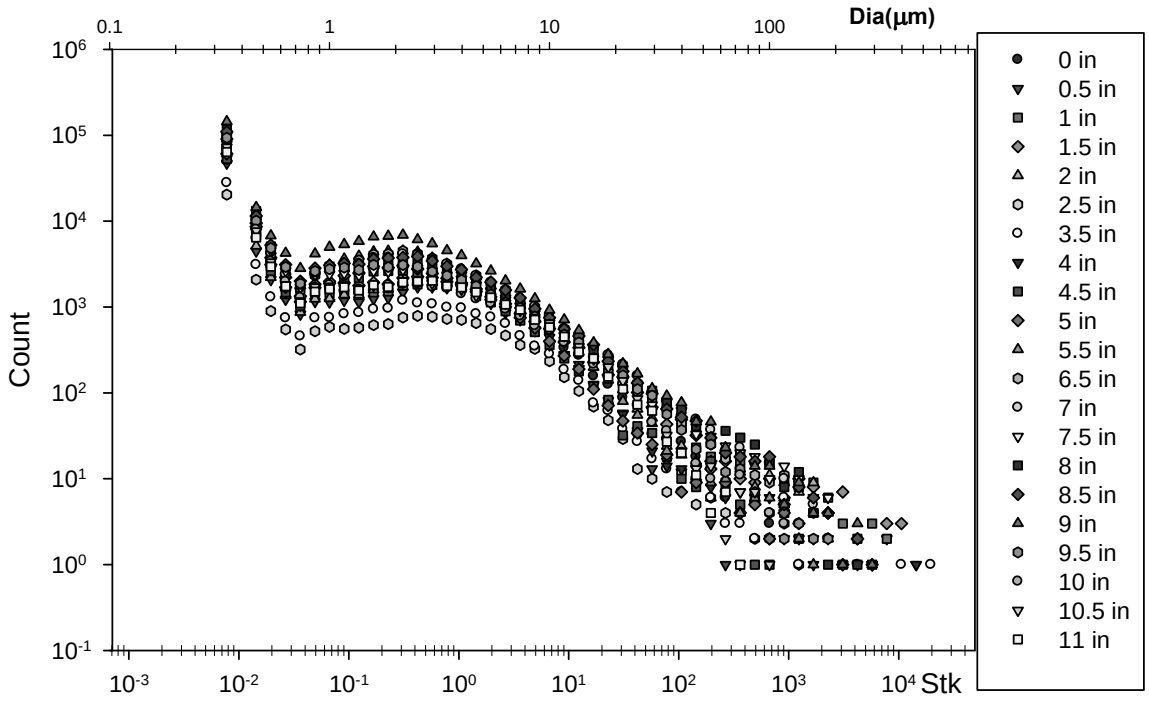

Fig. 2.7 - Particle distribution as a function of vertical position along the impactor plate

This analysis demonstrates that there is a significant variation in the number of particles along the impactor from top to bottom. The spread in the overall data covers roughly an order of magnitude, with the data collected at the 9" mark yielding the highest counts and at 2.5" the lowest. The rest of the datasets fall between these two marks in no discernable order. This variation shows that there is no real trend in count as a function of vertical position. Figure 2.8 below selects several particle sizes to demonstrate this arbitrary nature of the deposition along the impactor face.

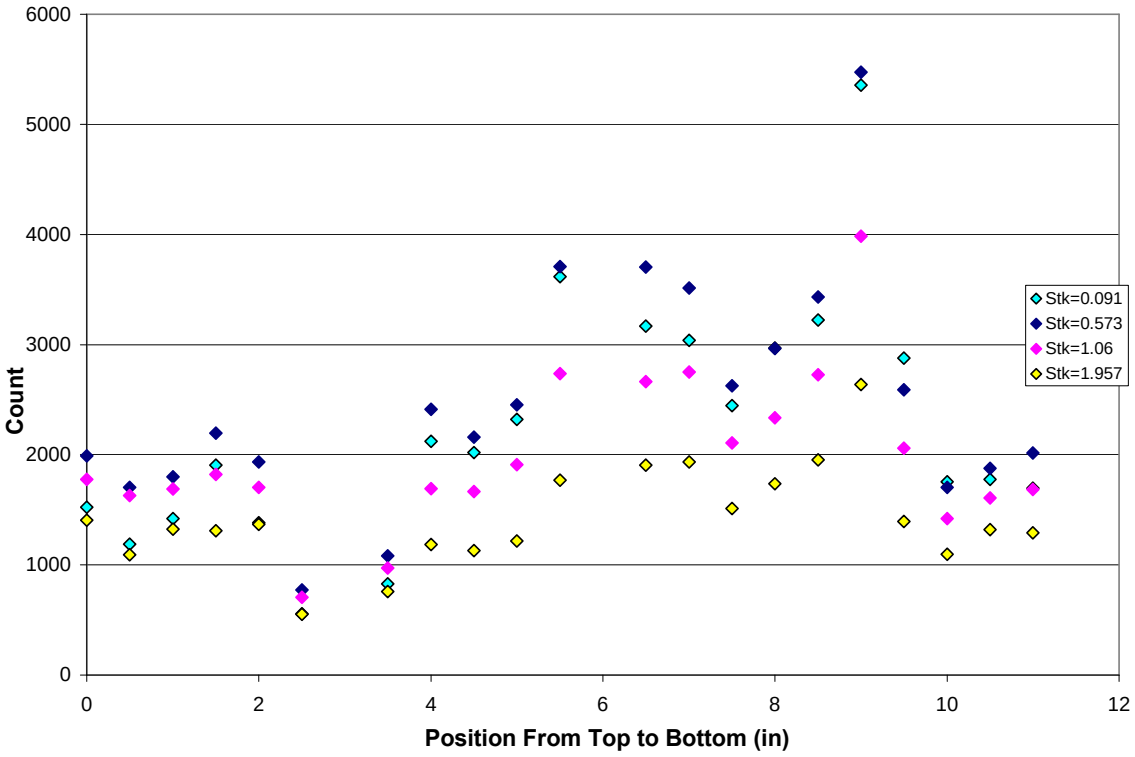

Fig. 2.8 - Particle count as a function of position along impactor plate for selected particle sizes

There are two noticeable locations of deviation from the general observed trend in the data. The dip at the 2.5" location and the peak at 9" were locations where two glass slides met. Neglecting these two obvious outliers, a trend can be seen out towards the edges with an increase in collected particles towards the center of plate. This establishes the empirical basis for the remainder of the testing to be conducted with fewer slides, centered on the face plate, without risking the loss of data fidelity.

2.3.3 – Variation of Collected Distribution Between Impactor Plates

The nature of the impactor geometry for this system is very unique. Based upon the thorough analysis and design iterations done by Volpe, an ideal geometry was generated for this impactor (5). In an effort to give the impactor a more practical front area but maintain effective area, the 3.0ft long impactor was divided into three 1.0ft sections. It was necessary to show that this design choice did not adversely affect the collection efficiency. Microscope slides were placed at the center of each impactor plate and a summation over the central 5.0mm width perpendicular to the long axis of the impactor

was taken to get a count of collected particles. The total particle counts for each impactor plate were measured and compared (Fig. 2.9.)

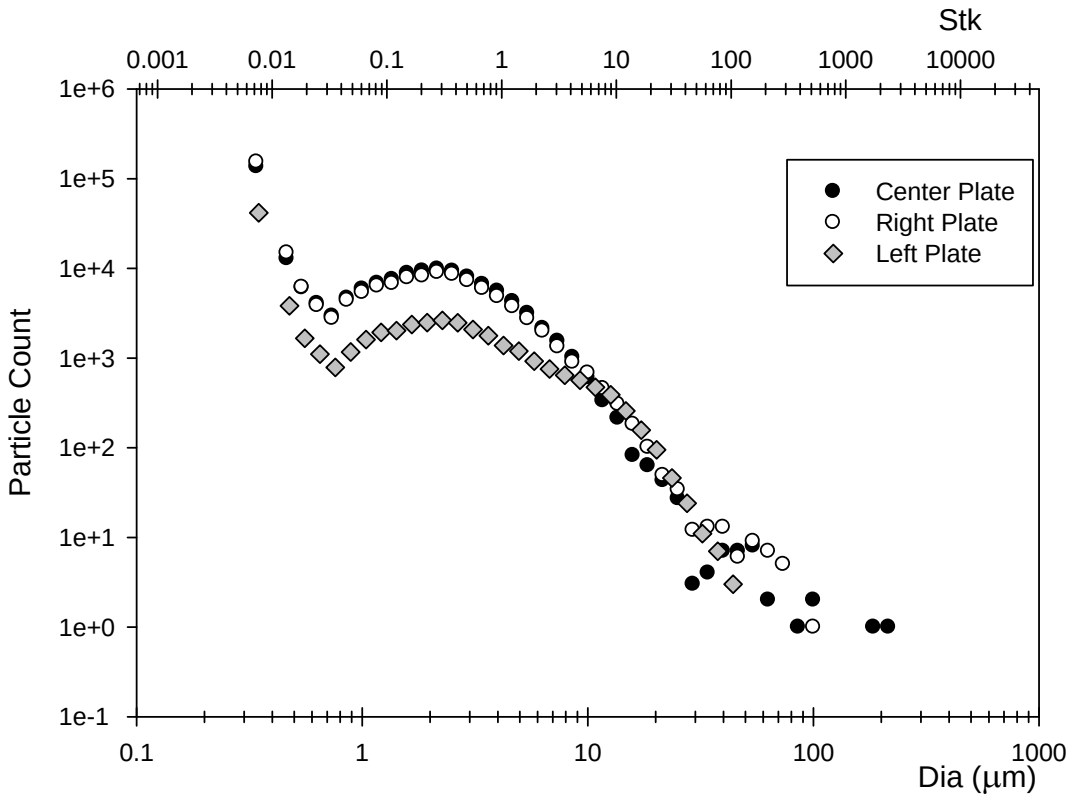

Fig. 2.9 - Plot of collected particle count as a function of Stokes number compared across impactor plates

This experiment demonstrates that there exists a noticeable bias away from the left plate. However, there is still significant-enough signal recorded to register a positive hit on an ion mobility spectrometer typically used in this type of screening process. The results from the experiment show that there are more than 1000 particles collected for each Stokes number in the range of sizes below Stk = 1.0. However, for Stk>1.0, a drop off of particle size is seen: hundreds of Stk~10 particles, tens of Stk~100 particles, etc, which is consistent with the anticipated size distribution of talc particles in the flow (Fig. 2.2.)

Based upon research conducted at the National Institute of Standards and Technology, a signal "hit" requirement for an ion mobility spectrometer is roughly 1000 particles for each of the three most common explosives at a diameter of approximately 1.0 μm (Fig. 2.10.)

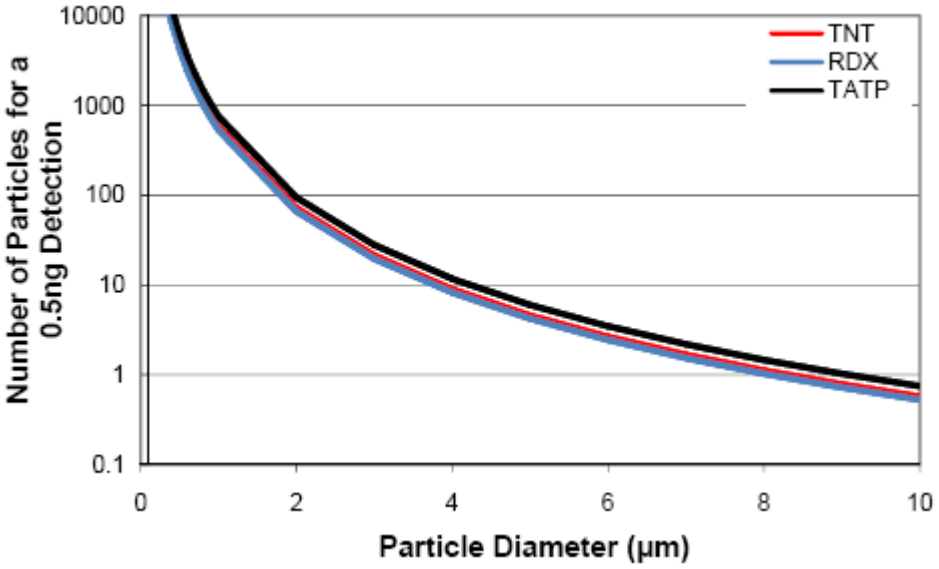

Fig. 2.10 - Number of particles required to record a 0.5ng explosive mass on an ion mobility spectrometer (5)

The table below shows the Stokes number of a 1.0 µm particle of the three listed explosives at the wake-sampling portal flow conditions. However, the impactor has been designed to have a cutoff at Stk = 1.0, meaning nothing smaller can be relied upon to generate a signal for analysis. Using the design point, the expected cut diameters of the explosives in question were calculated and tabulated below (Table 2.1.)

	Density (g/cc)	Stk @ Dia=1.0µm	Num @ Dia=1.0µm	Dia(µm) @ Stk=1	Num @ Stk=1
RDX	1.83	0.04128	~1000	4.922	<10
TNT	1.65	0.03722	~1000	5.184	<10
TATP	1.2	0.02707	~1000	6.078	<10

Table 2.1 – Density, relative Stokes number, and particle count of RDX, TNT, and TATP

From Table 2.1, the number of particles necessary to generate a signal at a Stokes number of 1.0 is less than 10. For all three impactor plates, the number of particles in this size range was well above the number required for the positive hit.

However, from what is seen in Fig. 2.9, there appears to be a preference towards the center of the impactors and away from the left plate. To confirm whether this was a result of the flow or experimental error, a hot-wire anemometer was used to measure the inlet flow velocity. The plane at the entrance to the impactor was divided into nine

sections and 25 readings were taken at the approximate center of each section. The results of this study are presented below in Fig. 2.11.

8.001m/s +/-0.0268	8.174m/s +/-0.0810	8.118m/s +/-0.0787
8.052m/s +/-0.0359	8.280m/s +/-0.0415	8.275m/s +/-0.0810
8.052m/s +/-0.0268	8.189m/s +/-0.0577	8.250m/s +/-0.0428

Fig. 2.11 – Flow velocity profile at impactor inlet plane

This experiment explains why the left-hand impactor appears to collect fewer particles than the center and right plates. For each vertical position, the average velocity at the impactor inlet is higher for the center and right impactor plates. As flow rate is directly related, this results in a higher Stokes number for all particles in the flow. Higher Stokes number increases the number and size range of particles that get collected. The same logic can be applied to the plates themselves when comparing particle counts vertically. The slight increase in flow velocity at the center of the plates returns a higher average particle count over the extreme top and bottom.

2.3.4 – Contraction Inlet Flow Separation Solutions

Based upon the results of the hot-wire anemometer survey of the impactor inlet plane, there was a significant difference in flow behavior from one side to the other. There appeared to be some phenomenon causing the flow to separate, thus stalling one side of the impactor. To confirm this hypothesis, two different experiments were conducted. Laser sheet and tufts flow visualization techniques were employed.

A laser sheet was set across the contraction inlet and theatrical fog was used to visualize the behavior of the flow at the critical location on the left-hand side of the inlet (Fig. 2.12.)

Fig. 2.12 – Left-hand side of contraction inlet with laser sheet illumination. Highlighted area is recirculation region.

This experiment confirms the hypothesis of a separated recirculation region on the left-hand side of the inlet. Fig. 2.12 clearly shows that the flow does not stay attached to the left wall as it enters the aerodynamic contraction due to the sharp corner. This, in turn, adversely affects the nature of the flow downstream at the impactor inlet and the effectiveness of the impactor.

The separation region is a result of the flow on the left-hand side having to make the turn around the sharp corner. The apparent solution to this problem was to install a fairing at the sharp corner. A cylindrical 10" diameter fairing was used to reduce the angle through which the flow has to turn to get to the impactor. This fairing reduced the separation region as evidenced by the fog pattern in Fig. 2.13.

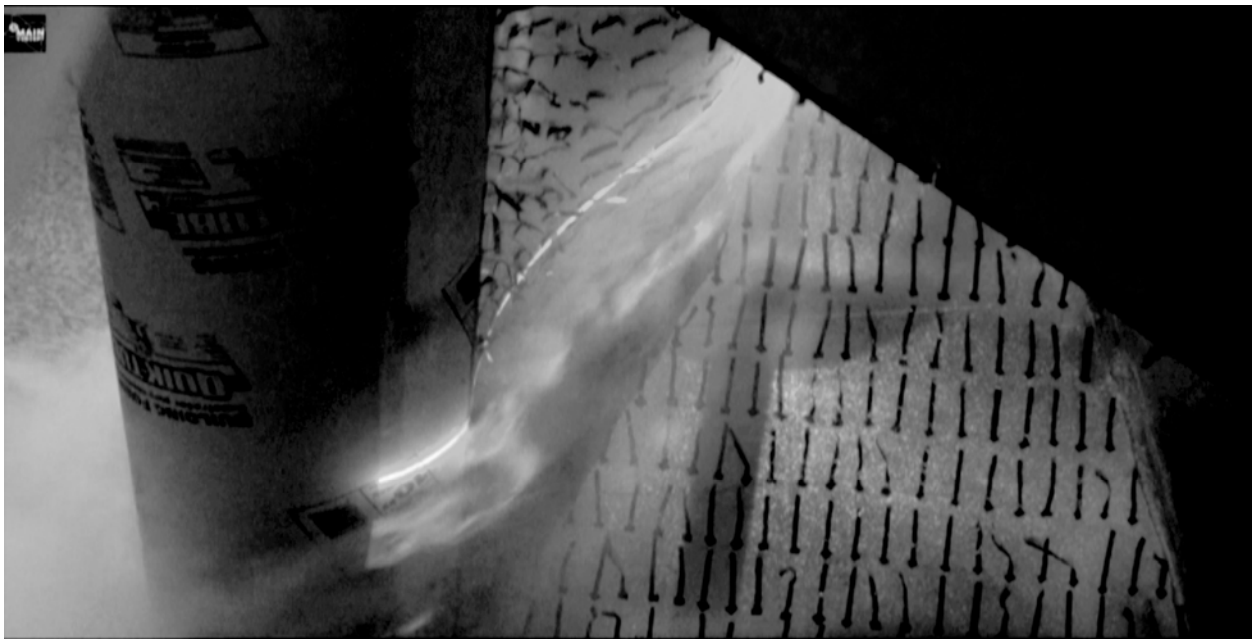

Fig. 2.13 – Left-hand side of contraction inlet with laser sheet illumination. 10" fairing installed showing no separation region

The fairing helps the flow to remain attached to the wall as it moves from the inlet into the aerodynamic contraction. The previous large recirculation is not present in this configuration, indicating that the majority of the bulk flow is no longer separated. Another experiment was required, however, to establish independent confirmation of the change in flow behavior.

The interior walls of the aerodynamic contraction were coated with ~2" long tufts made of a thin, plastic ribbon. These tufts were lightweight enough to be easily moved by the airflow. The unseparated flow keeps the tufts oriented in the main flow direction. A recirculation region causes the flow along the wall to be moving opposite to the direction of the bulk airflow, which is indicated by the tufts along the wall. By comparing the direction of the tufts before and after the installation of the fairing, it was possible to show that the separation region has been largely eliminated. The image sets below show the tufted walls with and without the fairing. The length of the separated region is indicated by the white dotted line (Figs. 2.14.-2.16.)

Fig. 2.14 – Top section of left-hand wall of aerodynamic contraction with wall-tuft flow visualization showing the effect of the installation of the 10" fairing on the recirculation region. Approximate flow separation locations shown by dotted white lines.

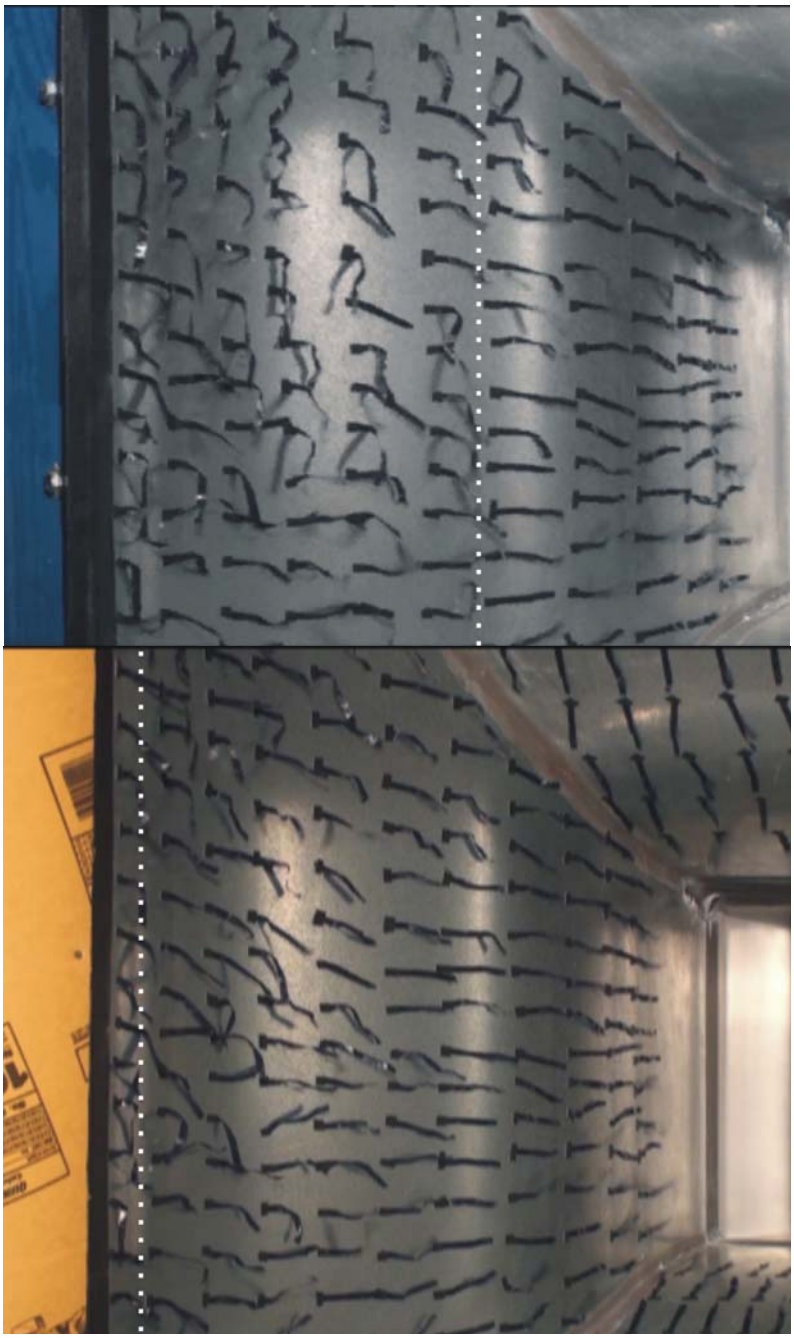

Fig. 2.15 – Middle section of left-hand wall of aerodynamic contraction with wall-tuft flow visualization showing the effect of the installation of the 10" fairing on the recirculation region. Approximate flow separation locations shown by dotted white lines.

Fig. 2.16 – Bottom section of left-hand wall of aerodynamic contraction with wall-tuft flow visualization showing the effect of the installation of the 10" fairing on the recirculation region Approximate flow separation locations shown by dotted white lines.

From each of the above images it is clear that the separation region has been significantly reduced with the addition of the 10" diameter fairing. There is still a very small recirculation region in the middle region, due to junction of the fairing and the aerodynamic contraction not being perfectly smooth. This slight variation causes a small

recirculation region that is believed to be inconsequential to the bulk airflow. The top and bottom walls have slightly larger regions of flow separation due to the end effects of the fairing and the corner between the side wall and the top and bottom of the contraction inlet. However, the size of the separation regions on the top and bottom portions of the left-hand wall has been notably decreased.

The next step was to determine the effect that this fairing had on the flow behavior at the impactor inlet plane. The same hot-film anemometer test conducted initially was repeated for this new flow geometry. The impactor inlet plane velocity was measured 25 times in the same grid pattern (Fig. 2.17.)

Avg(m/s) 8.280 StdDev(m/s) 0.047	Avg(m/s) 8.199 StdDev(m/s) 0.042	Avg(m/s) 8.184 StdDev(m/s) 0.028
Avg(m/s) 8.285 StdDev(m/s) 0.037	Avg(m/s) 8.225 StdDev(m/s) 0.044	Avg(m/s) 8.230 StdDev(m/s) 0.033
Avg(m/s) 8.291 StdDev(m/s) 0.032	Avg(m/s) 8.240 StdDev(m/s) 0.046	Avg(m/s) 8.260 StdDev(m/s) 0.026

Fig. 2.17 - Flow velocity profile at impactor inlet plane with 10" diameter fairing installed

This experiment shows a much-more-uniform distribution of velocity at the impactor face than what was seen in the initial test. From these results, it is clear that the fairing substantially solved the flow separation problem. There is less than 2% difference in the velocities across the impactor inlet, which results in a more even distribution of flow to the three impactor plates. The addition of the fairing should reduce the bias away from the left-hand impactor plate seen in Fig. 2.9.

Since the flow behavior was changed significantly due to the introduction of flow conditioning at the left-hand side of the inlet, flow visualization was employed to test the top and bottom edges of the contraction inlet. The same two methods, laser sheet (Fig. 2.18-2.19) and tuft (Fig. 2.20-2.21) visualization, were used to discover the nature of the flow along these edges.

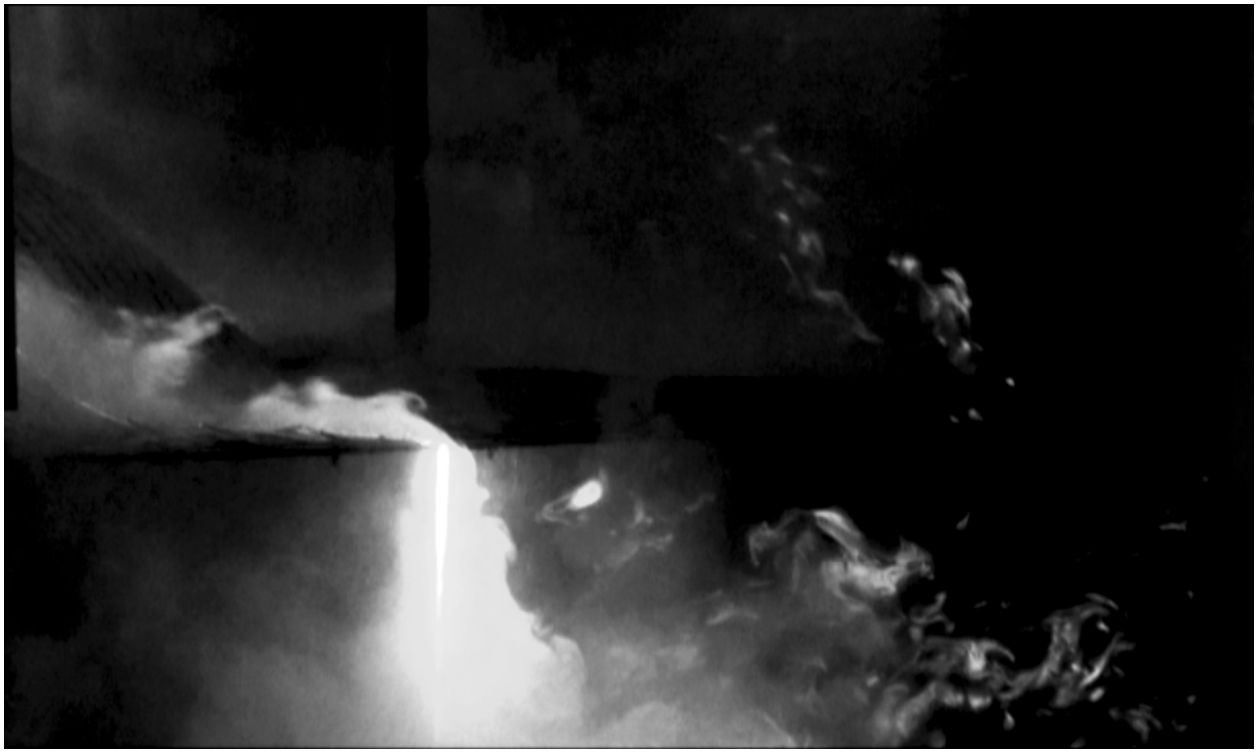

Fig. 2.18 – Laser sheet flow visualization of aerodynamic contraction inlet, bottom edge

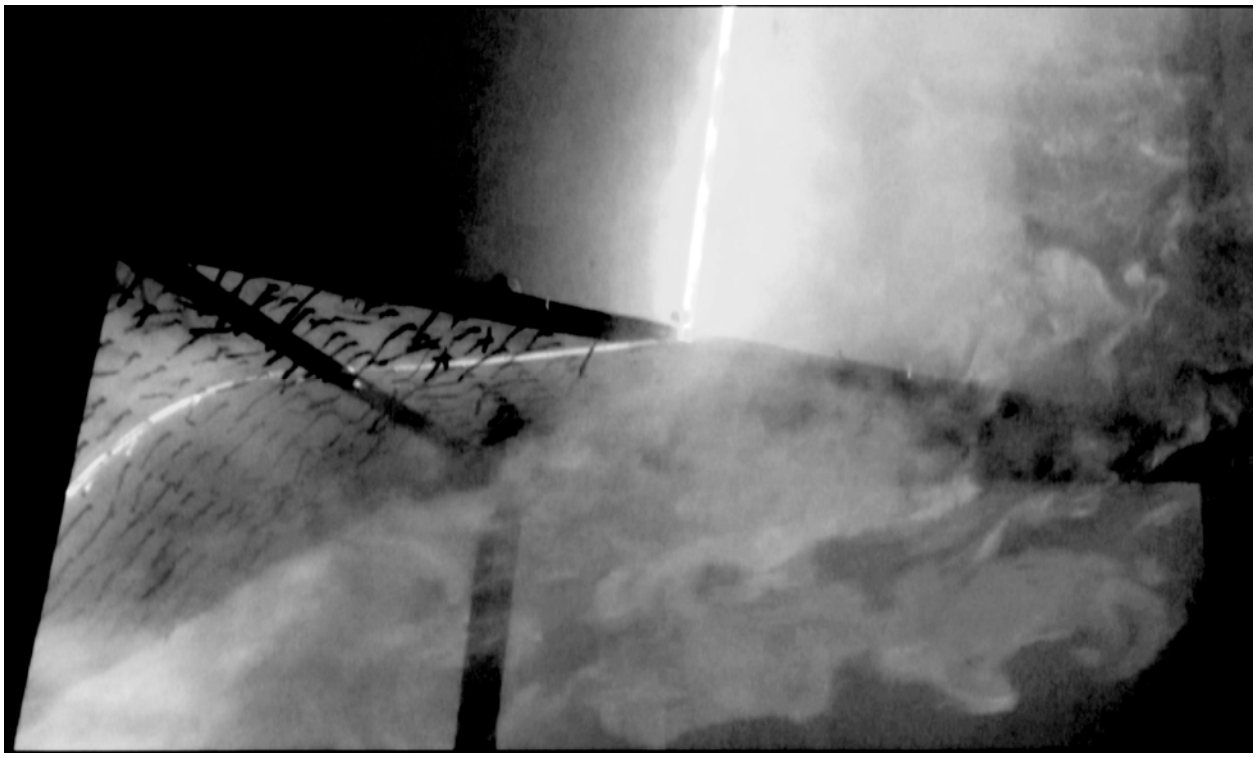

Fig. 2.19 – Laser sheet flow visualization of aerodynamic contraction inlet, top edge

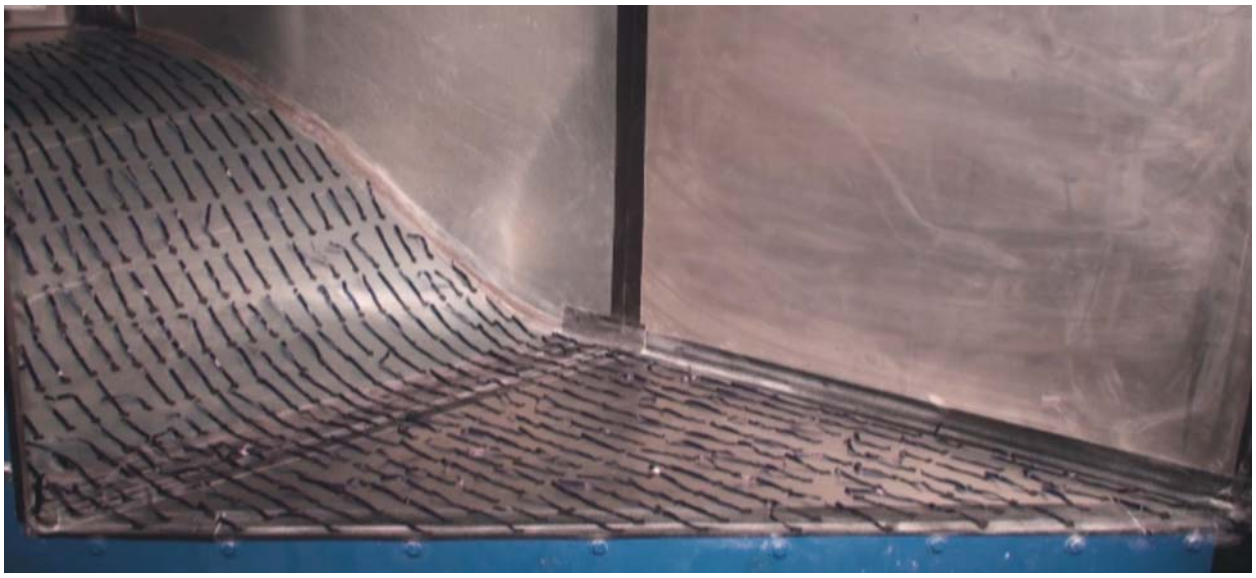

Fig. 2.20 – Wall-tufted flow visualization, bottom wall

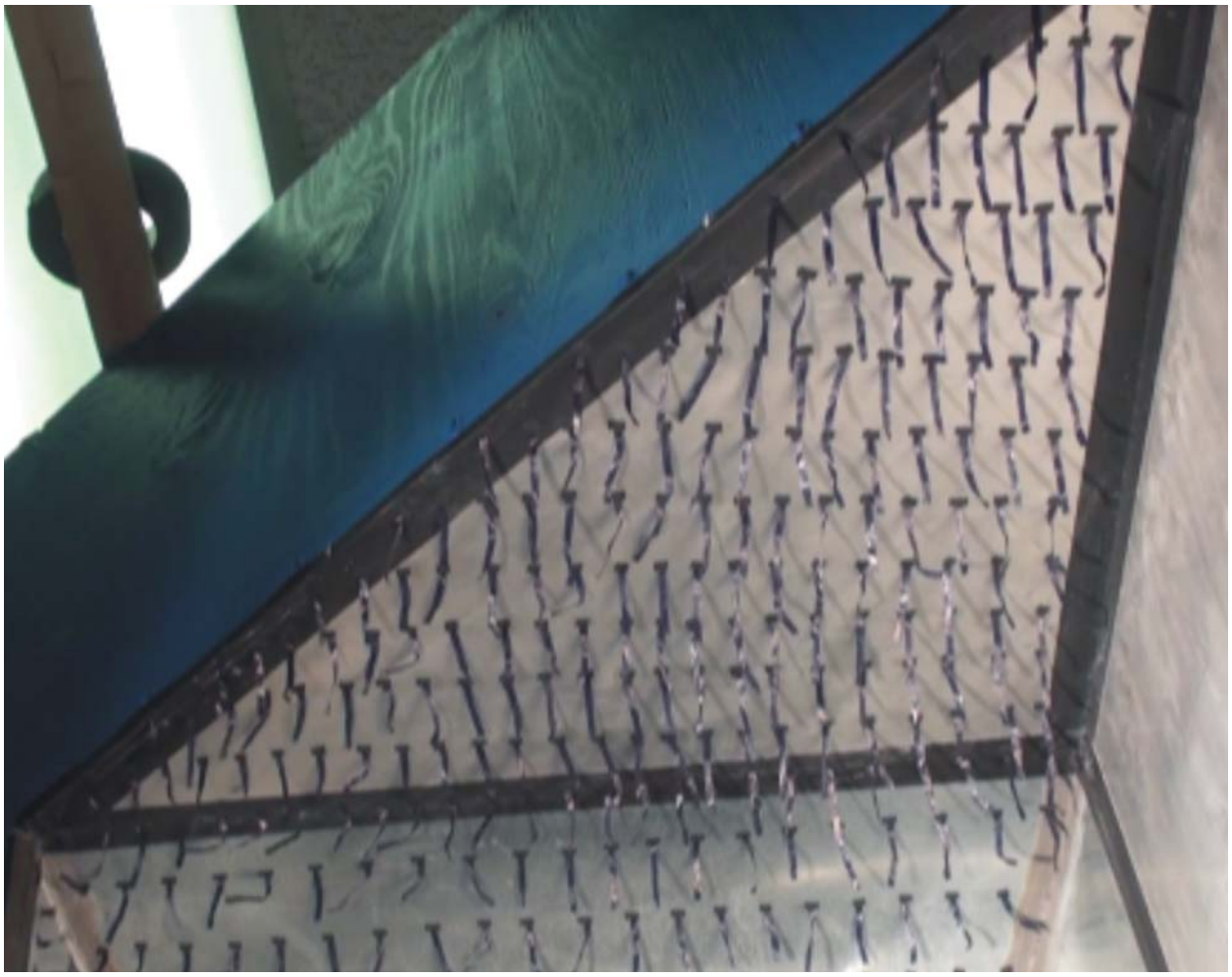

Fig. 2.21 - Wall-tufted flow visualization, top wall

These experiments show that the flow has no appreciable separation regions along the top and bottom walls. From the laser sheets seen in figures 2.18 and 2.19, it is clear that there is no separation at the top and bottom edges. The fog remains attached along the walls from the orifice inlet plane until it reaches the impactor inlet, where visualization is lost. The tufts along the top and bottom walls also reflect this result. There is virtually no evidence of a recirculation zone in any region along the top or bottom walls, where the tufts are oriented in the main flow directions at all locations.

To confirm that the weight of the tufts was not holding them down to the wall in defiance of the flow characteristics, the tufts were prepositioned with their tails against the stream. The bulk airflow immediately shifted the tufts into the streamwise direction, eliminating tuft weight as a source of error.

These experiments conclusively demonstrate that there are no longer any areas of separated flow along the inlet edges of the aerodynamic contraction. The two independently-conducted experiments confirm that the separation region initially present along the left-hand inlet edge has been significantly reduced. A hot-film anemometer survey concluded that there was an improvement in the uniformity of the flow at the impactor inlet plane compared to the initial portal geometry, thereby minimizing the collection bias away from the left-hand impactor plate.

To confirm the elimination of the flow bias, the talc deposition test previously done to compare the collection on each of the three impactors was reconducted. Ten tests were run with the same experimental setup used before. Aerosolized talc was introduced via the fluidized bed for collection on the impactor faces. The original intent of this experiment was to demonstrate that there was no longer a rightward bias in trace collection by counting the particles deposited on the glass slides. However, a count was unnecessary as it was possible to determine that the rightward bias was still present by visual inspection of the impactor faces. On each of the images below, there are bright white lines on each impactor face that indicate the deposition of talc (Fig. 2.22.)

Fig. 2.22 – Images of 10 talc-deposition tests processed to highlight talc deposition.

It is clear from the majority of the tests seen in this image that there is still some bias in the collection characteristics of the wake sampling portal. Most of the runs show no collection on the left-hand impactor plate. Those that do, runs 3, 4, and 9, show a significantly-higher concentration of particles on the center and right-hand impactor plates. Previous experiments show that the effects of separation regions present at the contraction inlet have been reduced and that the velocity field at the impactor inlet plane

is nearly uniform. This indicates that there is some other factor influencing the flow to create this undesirable biasing.

The flow of particles to be collected and interrogated was introduced as a large-volume aerosol-containing region several meters upstream of the impactor and the aerodynamic contraction. It was hypothesized that the bias may have been introduced due to problems in this particle delivery method. If the particle stream was not centered and uniformly spread throughout the total range of the bulk airflow, it could explain why there was a significantly-different signal level across the three impactor plates. Laser sheet flow visualization was again employed to illustrate the flow field entering the contraction (Fig. 2.23.)

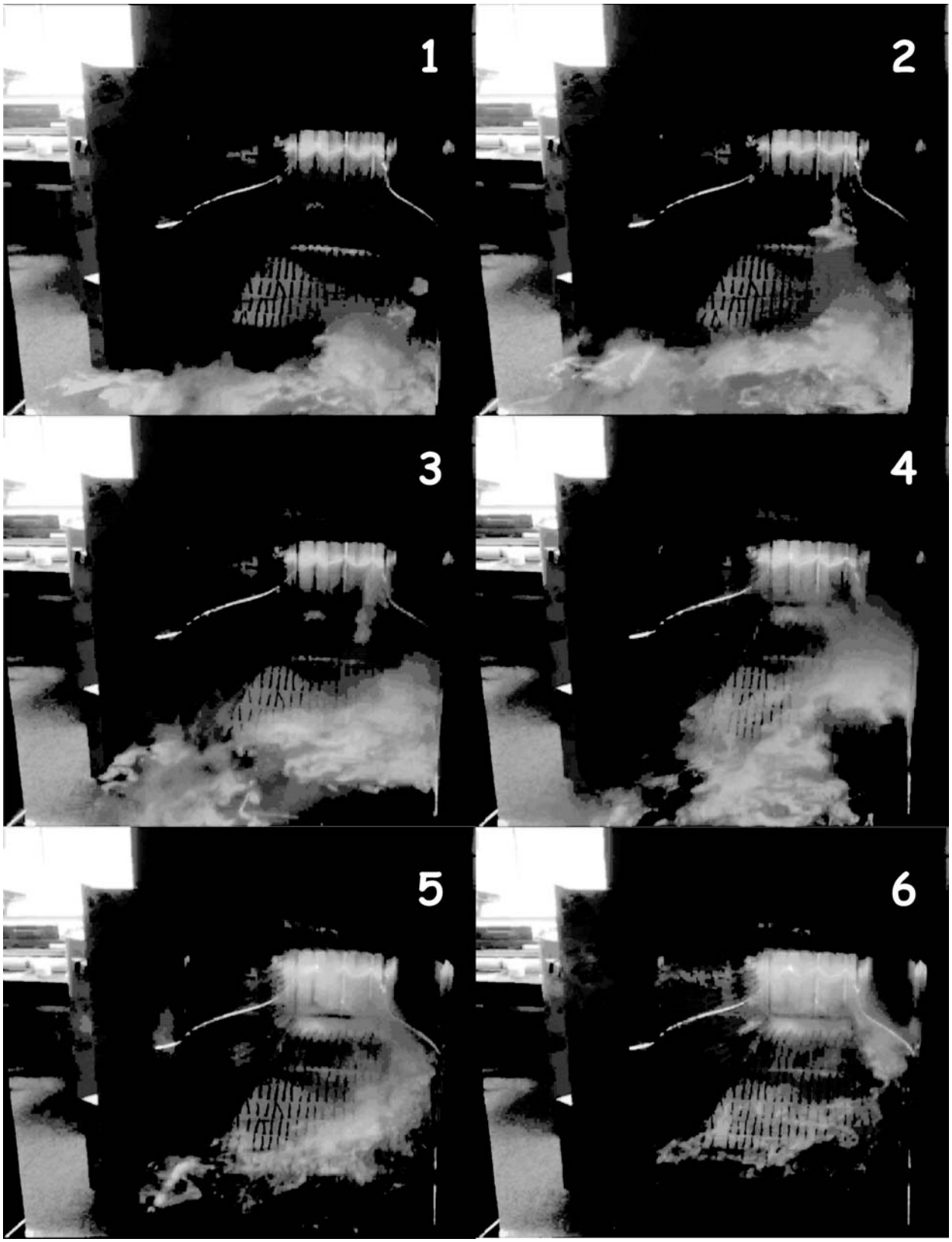

Fig. 2.23 – Series of 6 images showing the right-hand bias of a puff of theatrical fog introduced uniformly at the inlet to the aerodynamic wake sampling portal.

The series of images in Fig. 2.23 show that, despite a cloud of fog being introduced to the portal entrance uniformly, the flow shows a clear preference to the right-hand side of the aerodynamic contraction and impactor. Since the presence of a bias inside the contraction and impactor has been clearly disproven, the bias must be introduced by factors external to the aerodynamic wake sampling portal.

The ultimate outlet of the portal currently vents into the room containing the portal. This generates a very slight air current that circulates through the room from portal exit to entrance. There are heating, ventilation, and air conditioning (HVAC) vents in the ceiling that also move air through the room, contributing to the low-power, room-scale flow patterns. These two factors combine to generate a crossflow that is strong enough to vector the fog and the lightweight talc particles slightly towards the right-hand, protected side of the portal. To counteract this effect, it is recommended that these portals be installed far enough away from the HVAC vents that their effects will not influence the flow entering the impactor. Furthermore, the diffuser used at the blower outlet must be ducted out of the airspace that the portal resides in, and makeup air must be provided.

Eliminating this room-scale recirculation region will allow for a more uniform deposition across the three impactor plates, increasing the effectiveness of the portal and the ease of use for screening airline passengers.

2.3.5 – Collected Particle Distribution across Impactor Face

The final step of the collection experiments was to establish a particle size distribution laterally across the impactor face. It has clearly been shown that particles of a wide size range are collected on the impactor, with a concentration on the vertical centerline of each impactor plate. To cover the entire width of the impactor face, 2” by 3” microscope glass slides were centered on the impactor. The fluidized bed described earlier generated the particle flow, which was collected and analyzed using MATLAB (Fig. 2.24.)

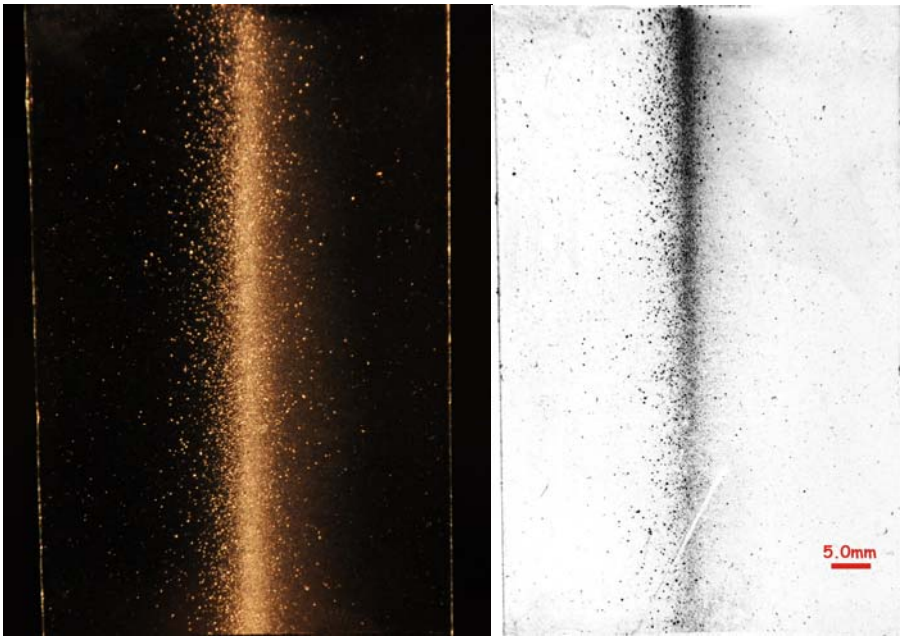

Fig. 2.24 – 2" slide with collected particles, raw image (left), processed image (right)

This image clearly shows the concentration of most of the particles around the centerline, with a few visible larger particles scattered across the rest of the impactor face. Images were taken across the slide to establish the size distribution as a function of the lateral position across the impactor plate. These particle counts were averaged over the vertical height of the slide and the size distribution was determined (Fig. 2.25).

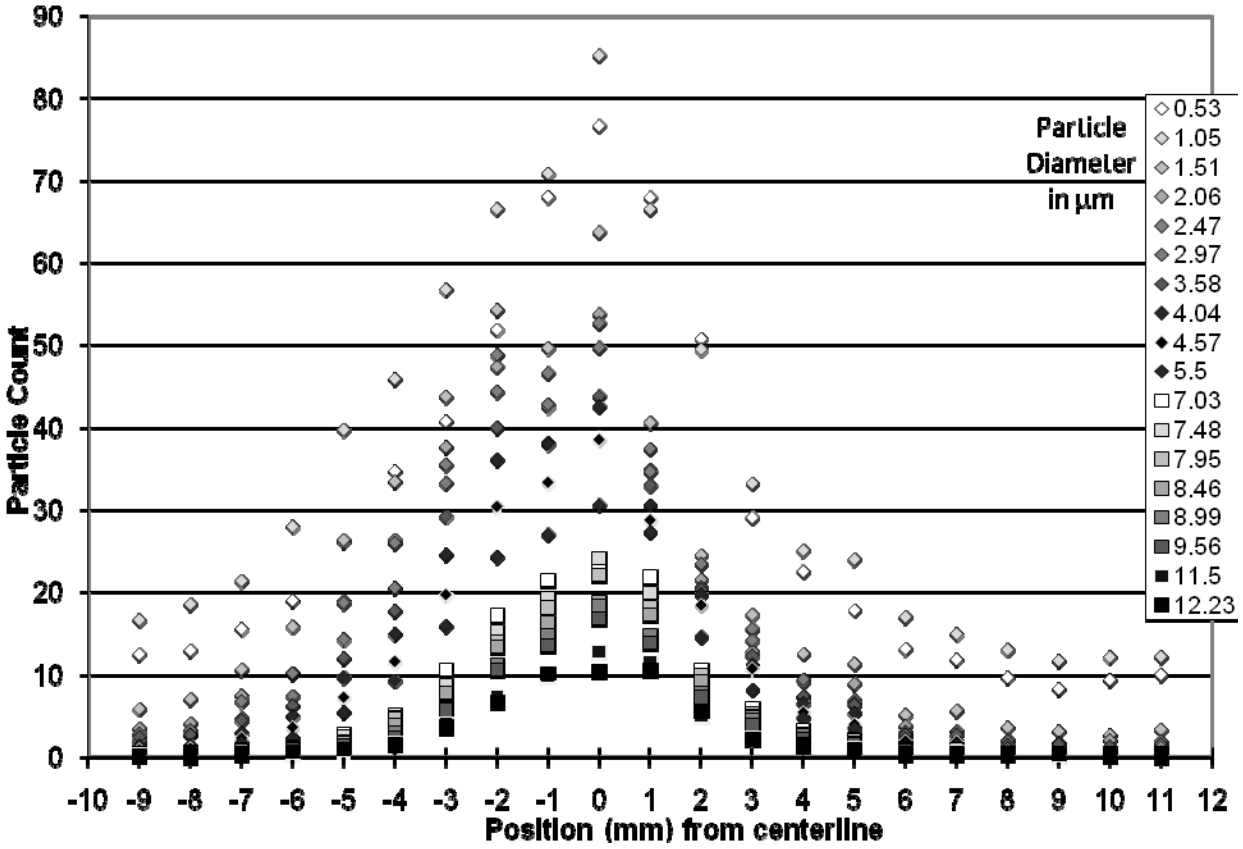

Fig. 2.25 – Sample of the particle distribution across the impactor plate

It is clear that there is an approximately normal distribution of particles across the face of the impactor plate. To see this more clearly, samples of particle sizes less than, approximately equivalent to, and larger than the cutoff diameter were taken and compared (Fig. 2.26.) These sizes were chosen to reflect the general behavior of the particles above and below the design cutoff diameter of the impactor.

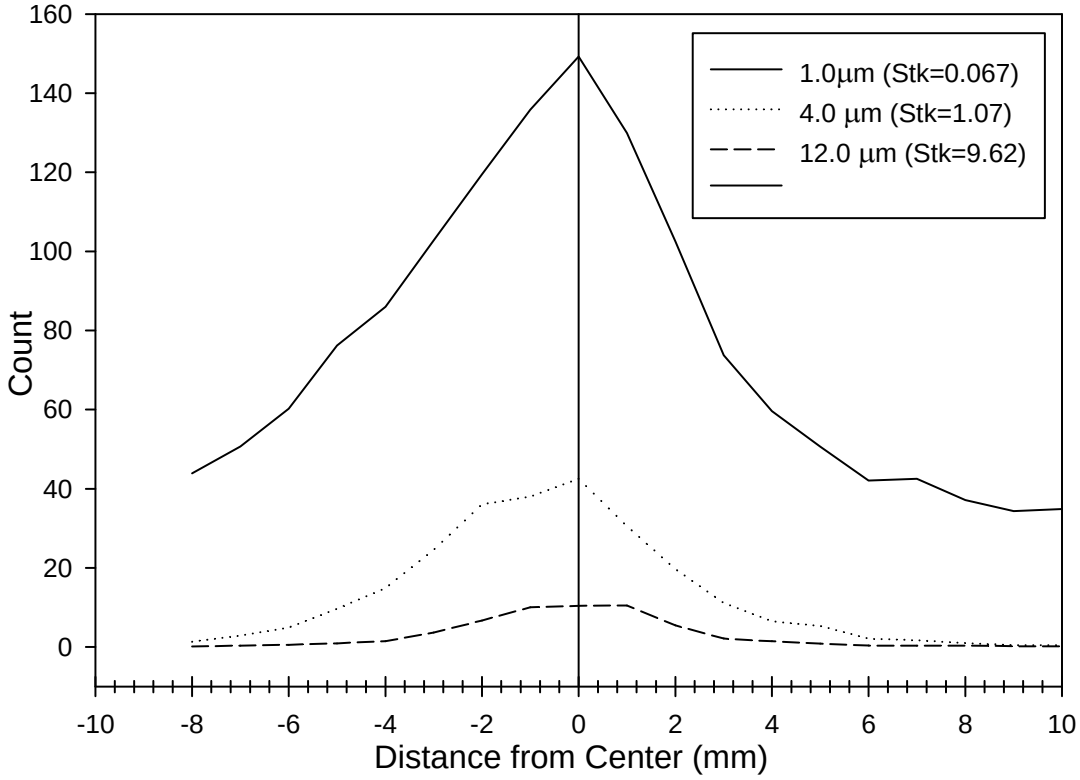

Fig. 2.26 – Collection locations for particle sizes below, equal to, and above the cutoff diameter

From this more-focused plot, it is evident that the range of impact locations narrows as particle size increases. Particle diameters below the cutoff can impact anywhere across the face of the impactor, while those at or above the target 4.0 µm are collected closer to the centerline of the impactor. The particles of 4.0 µm impact 5-7mm from the centerline, while the 12.0 µm particles are collected only 3-4 mm from the centerline. This is important information for the future development of a more effective collection/desorption method, such as a collection substrate or grooving. By knowing where the majority of target particles will be collected, these tools can be implemented more effectively and trace materials can be collected more efficiently.

2.4 – Computational Analysis of Particle Collection

To confirm the collection results seen in the microscope tests, a computational analysis was conducted with the FLUENT model used for the streamline-design of the impactor. The fully-resolved flow solution was employed to trace particle pathlines from the jet inlet to either the impactor faceplate or to the exit of the impactor. Since the flow upstream is considered to be uniform in this simulation, it was possible to focus the

analysis on just a single jet/impactor pair and have it represent the behavior of the entire impactor (Fig. 2.27.)

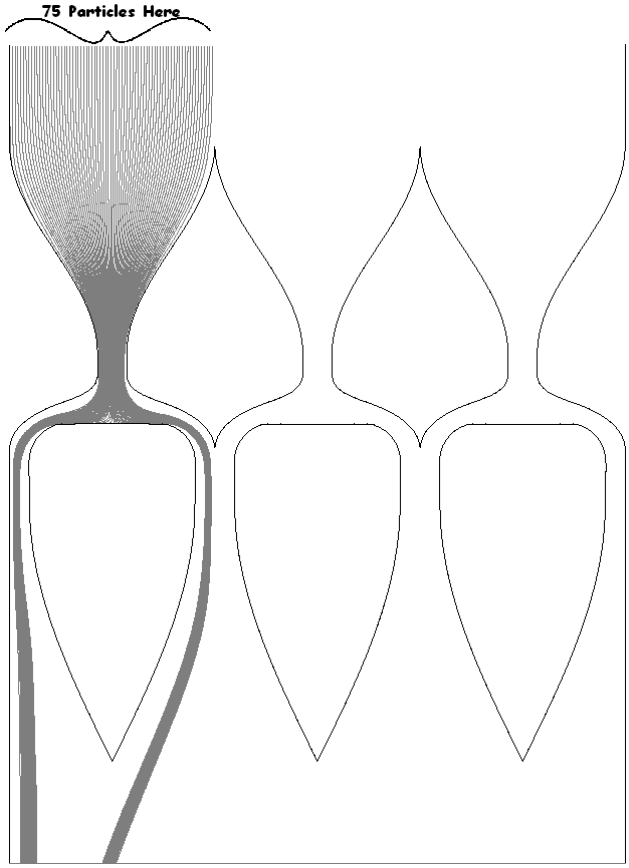

Fig. 2.27 – FLUENT impactor model with particles introduced at one inlet

2.4.1 – Computational Analysis of Particle Impact Location

75 evenly-spaced particles, simulated as talc with $\rho = 2.8$ g/cc, were introduced into the impactor across the inlet. Each streamline trace computation was conducted with a single particle diameter, starting with particles of 0.5 μm and going up to 20.0 μm. The number of particles whose final position was on the impactor face was recorded and a collection efficiency curve was generated. The final position across the impactor of the collected particles was also measured to determine the collection distribution for comparison with the microscopic experimental data (Fig. 2.28.)

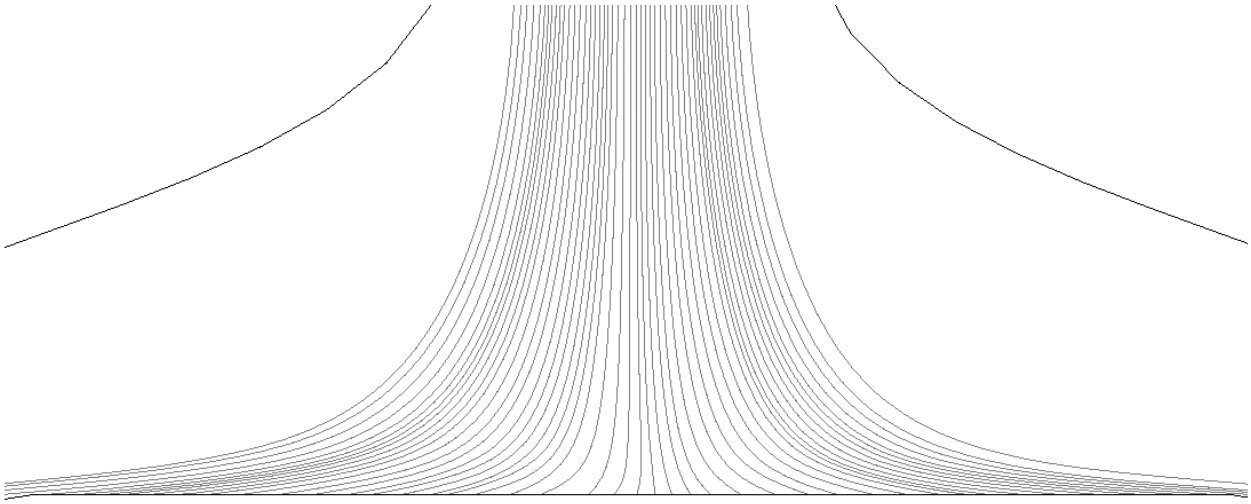

Fig. 2.28 – Example image used to record particle trace terminal points

As seen in the microscope tests, the range of particle impact locations narrows with the increase of particle diameter. Since this is the case, the measurement of the overall range of impact locations is chosen in favor of individual particle locations. The ranges of particle impact (horizontal axis) were plotted as a function of the particle diameter (vertical axis) in Fig. 2.29. The same trend observed in the microscopic analysis of impacted particles was also reflected computationally.

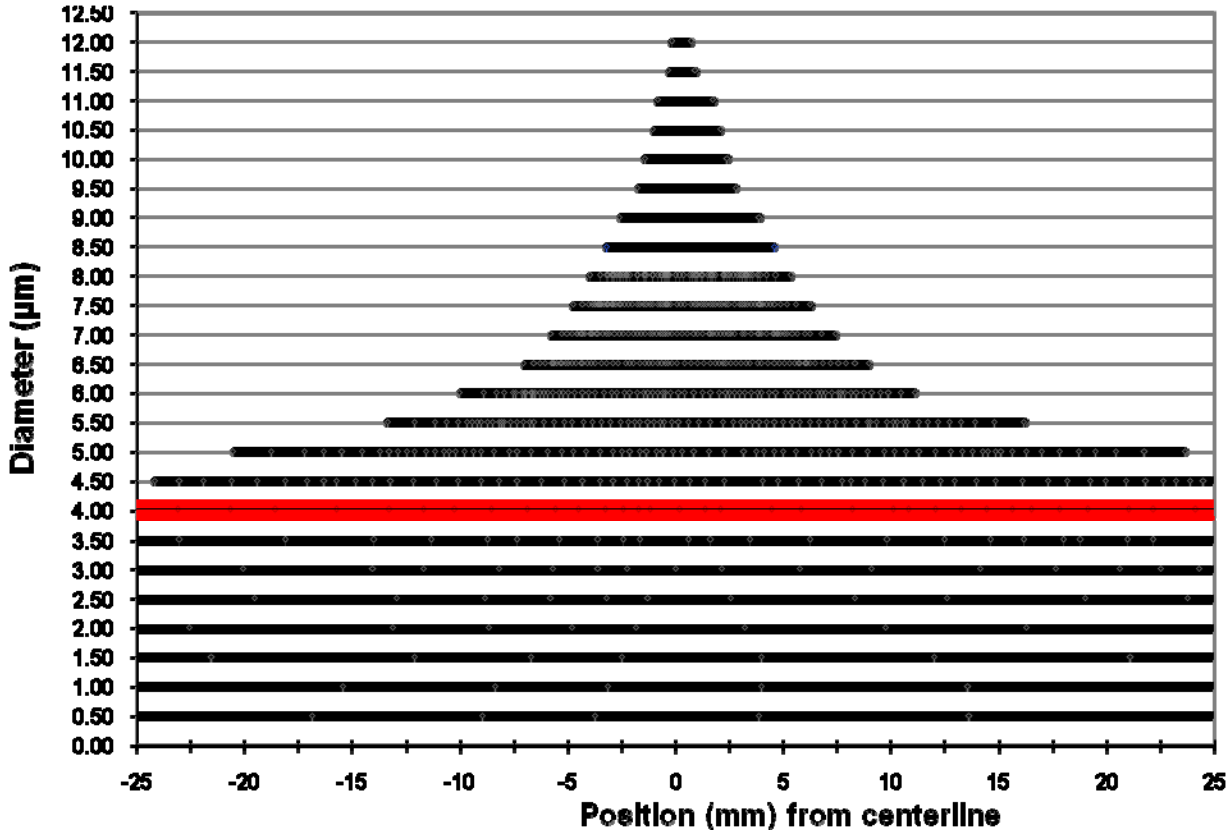

Fig. 2.29 – Range of impact locations as a function of particle diameter, from computational analysis

From this analysis, it is clear that the same general trend is observed. Particles below the cutoff size, the thick red line in Fig. 2.29, impact across the entire width of the impactor plate. As the particle diameter reaches and exceeds the cutoff diameter, the size of the impact region narrows with the increase in particle diameter. The cut does appear to be more sudden and more extreme than what was seen in the empirical case, as would be expected given the idealized conditions of the computation. However, when compared directly, it is clear that the results from the experiment and computation support one another and a confident conclusion can be drawn (Fig. 2.30.)

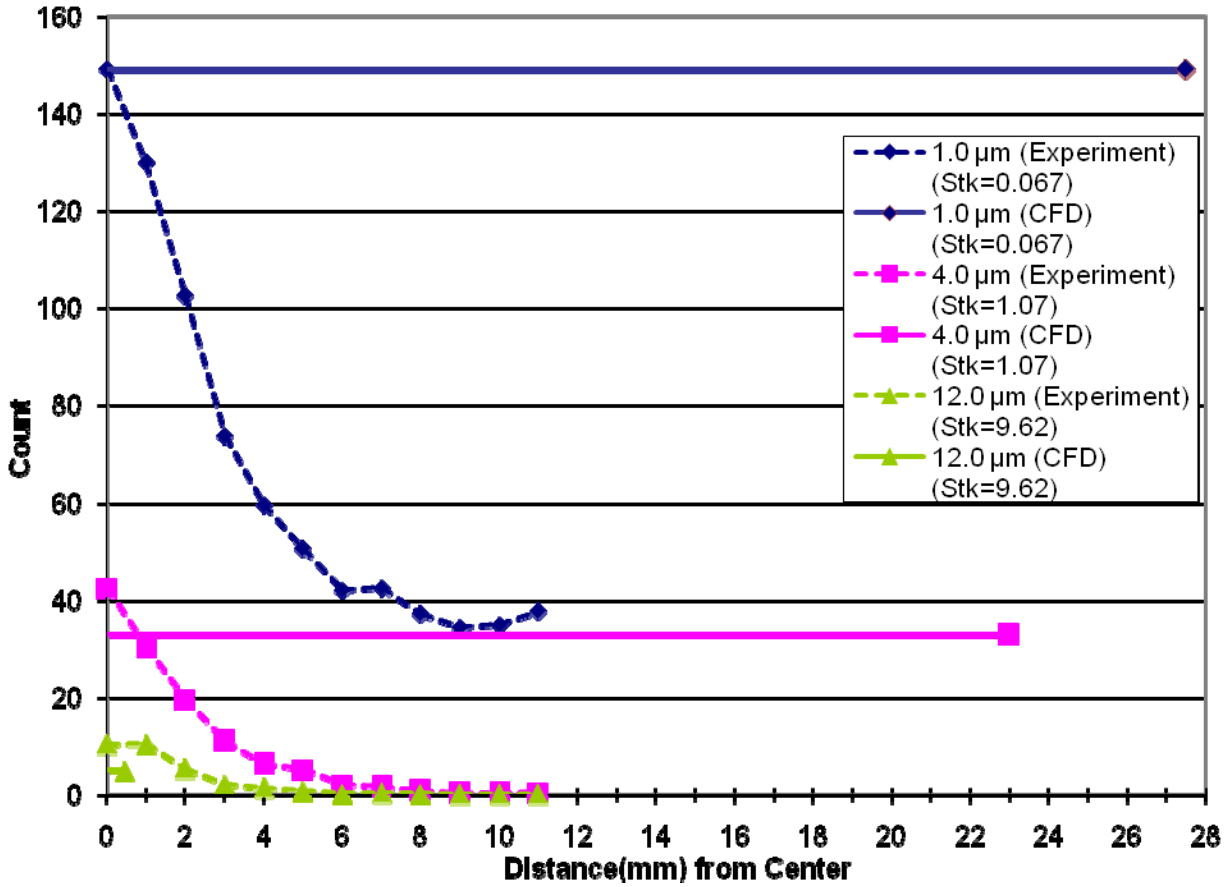

Fig. 2.30 – Particle impact ranges from experimental and computational results

It is clear that there is similar behavior from both experiment and computation. However, there is a significant change in the degree that the cutoff diameter affects the overall impact range between the two experiments. While the diameters below the cutoff impact across the entire impactor in both cases, the collection ranges above the cutoff vary greatly. The ~4.0 µm particles were deposited in the central 50mm in the computation versus the central 10mm in the experimental case, indicating that the actual impactor is performing better than expected at this particle size range. The ~12 µm particles behave quite differently, however. In this case, the experimental model shows particle collection within 4mm from the centerline and the computational model performs much better, collecting within ~0.5mm.

Despite the lack of direct correlation between the two experiments, the trends are consistent. This is a strong indicator of the overall effectiveness of the impactor at

removing and concentrating the particles at the center of the impactor plate for targeted investigation.

2.4.2 – Computational Determination of Impactor Efficiency

Because the number of particles introduced into the impactor was known, it was possible to generate a collection efficiency curve by obtaining the ratio of collected particles to introduced particles. This curve had the standard S-shape and showed the 50% cutoff diameter to be at Stk~1, per the design point (Fig. 2.31.)

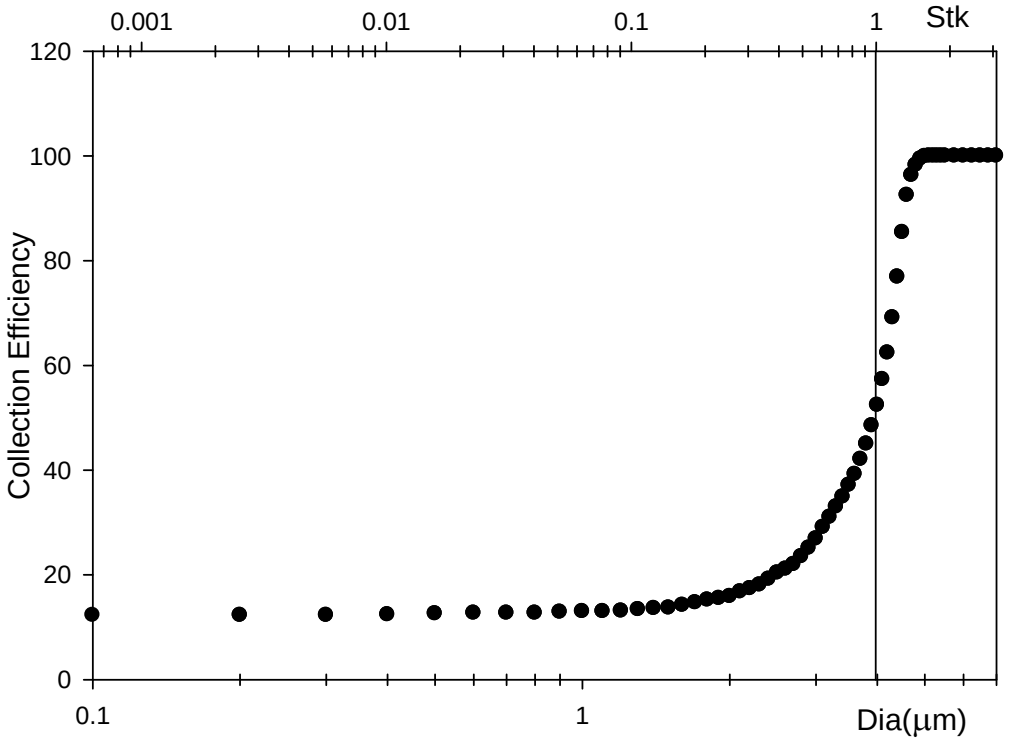

Fig. 2.31 – Efficiency curve determined from computational model particle traces

This demonstrates that, computationally, the impactor operates as expected based upon the design. The actual impactor will not likely have such ideal conditions: mono-dispersed particles, uniform distribution at the jet inlet, no particle interaction in the flow or on the impactor plate, no particle roll-off, and a known number of particles introduced to the flow. As a result, the real efficiency is anticipated to be marginally diminished from this ideal computed case, moving the 50% cutoff point to a slightly higher Stokes number.

2.5 – Particle Distribution Study

The experiments conducted with the microscope slides showed that the impactors do remove particles from the bulk airflow. The computational analysis of particle collection provided an equivalent picture of particle removal, as well as an impactor efficiency curve. An additional experiment was necessary, however, to determine how the collected particle size distribution related to the introduced particle size distribution. To conduct this experiment, the particle size distribution without the impactor plates in position needed to be established first. This baseline case would then be compared to the particle distribution measured with the impactor plates removing the target particle sizes from the bulk flow. The change would indicate the level of particle removal from the distribution that was introduced upstream, generating a measure of efficiency for the impactor.

2.5.1 –A Description of Fraunhofer Diffraction and Experimental Setup

The Malvern SprayTec particle sizer works on the principle of Fraunhofer diffraction (Fig. 2.32.)

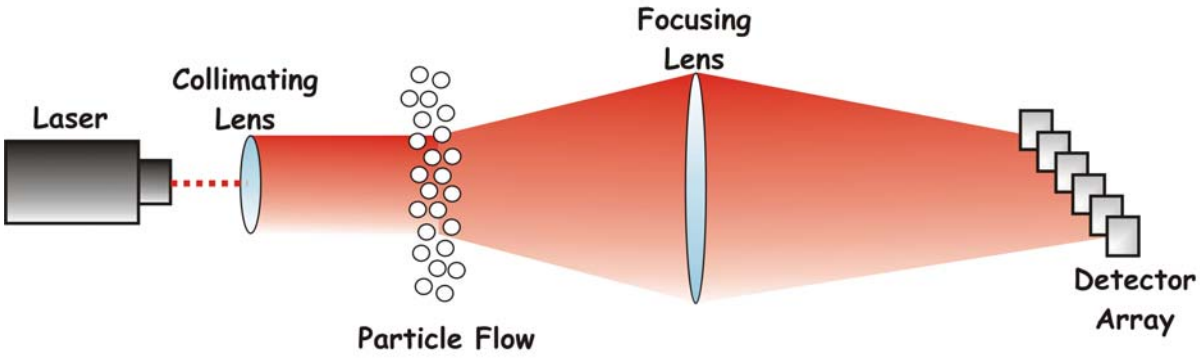

Fig. 2.32 – Diagram of a Fraunhofer diffraction setup

Light is emitted from the laser and expanded into a wide band of parallel light by the collimating lens or beam expander. The light then impacts the particle flow and, depending on the size and material of the particle, is diffracted through a certain angle. The focusing lens collects the diffracted light and concentrates it back down to the detector array, concentrating the unaffected light to a dead spot that does not influence the signal seen by the detectors. Each of these detectors is set to collect light shifted through a certain range of angles, and to generate a signal according to the fraction of the

flow that corresponds to particles of that size (10). The data from this type of experiment are generally presented in terms of a volume as a function of particle diameter (Fig. 2.33.)

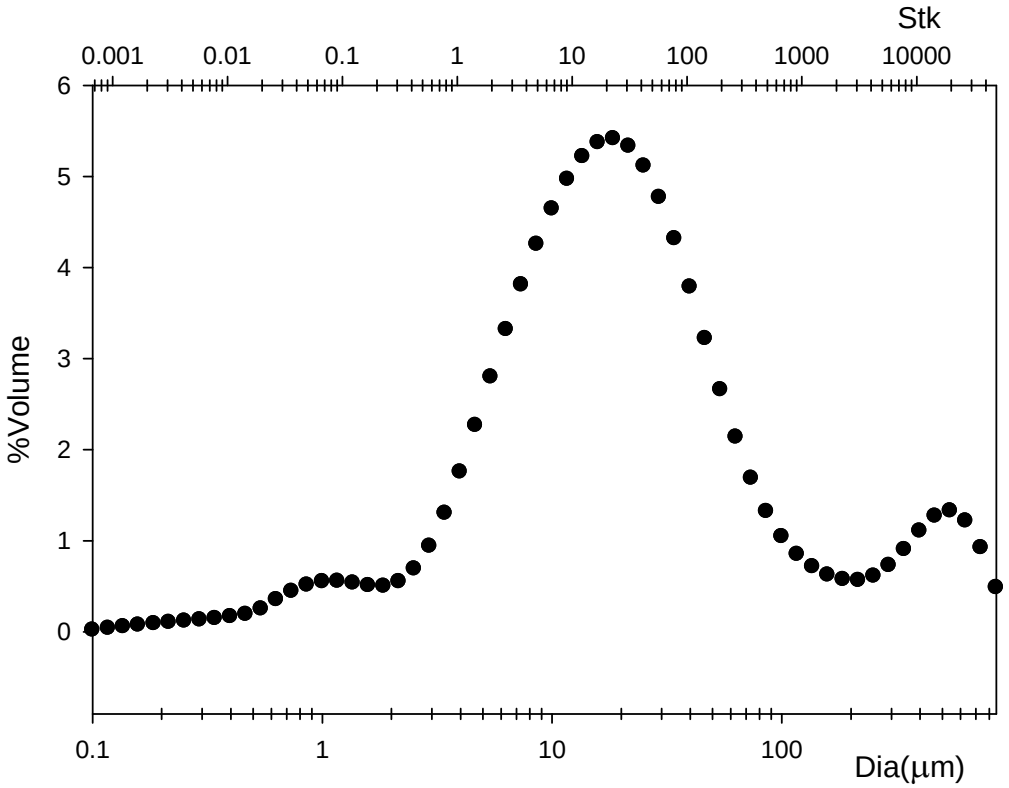

Fig. 2.33 – Sample output from a Fraunhofer diffraction analysis of particle size

To implement this technology in investigating this particle flow, the Malvern particle sizer was positioned downstream of the impactor to measure the particle distributions (Fig. 2.34) This site enabled readings to be taken without any effect on the flow transporting particles to the impactor.

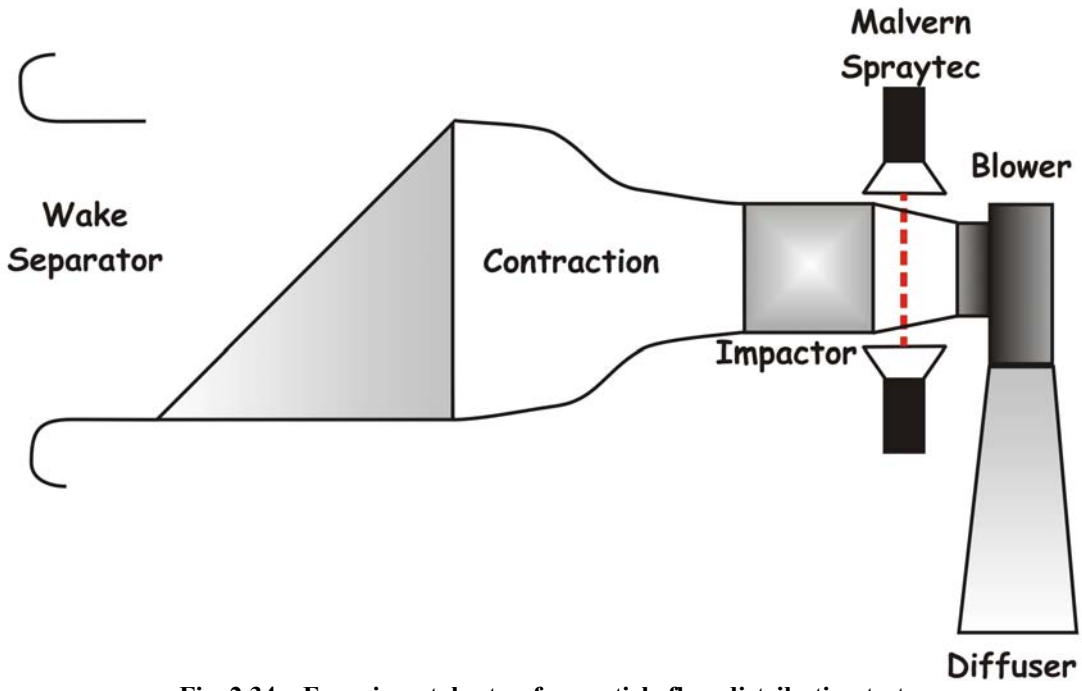

Fig. 2.34 – Experimental setup for particle flow distribution tests

For this experiment the Malvern instrument would need to be firing its laser through a glass-covered hole cut in the ducting between the impactor and the blower. It was necessary to establish that using the Malvern in this manner would not affect the results. The glass, necessary to seal the optical access holes and maintain the flow rate at the impactor face, could diffract the light if not perfectly perpendicular to the laser axis. Also, since the tests were being conducted through a hole, there was the risk of the diffracted beams being clipped by the edges of the hole and that signal being lost. Finally, the experiment would have to be conducted with the entire apparatus upside-down from its standard orientation due to the geometry of the impactor-blower assembly.

2.5.2 – Malvern Test: Analysis of Particle Distribution through a Hole

Before cutting holes in the breadboard portal, simplified tests were conducted using cardboard squares set 1 foot apart to mimic the geometry of the ducting behind the impactor (Fig. 2.35.)

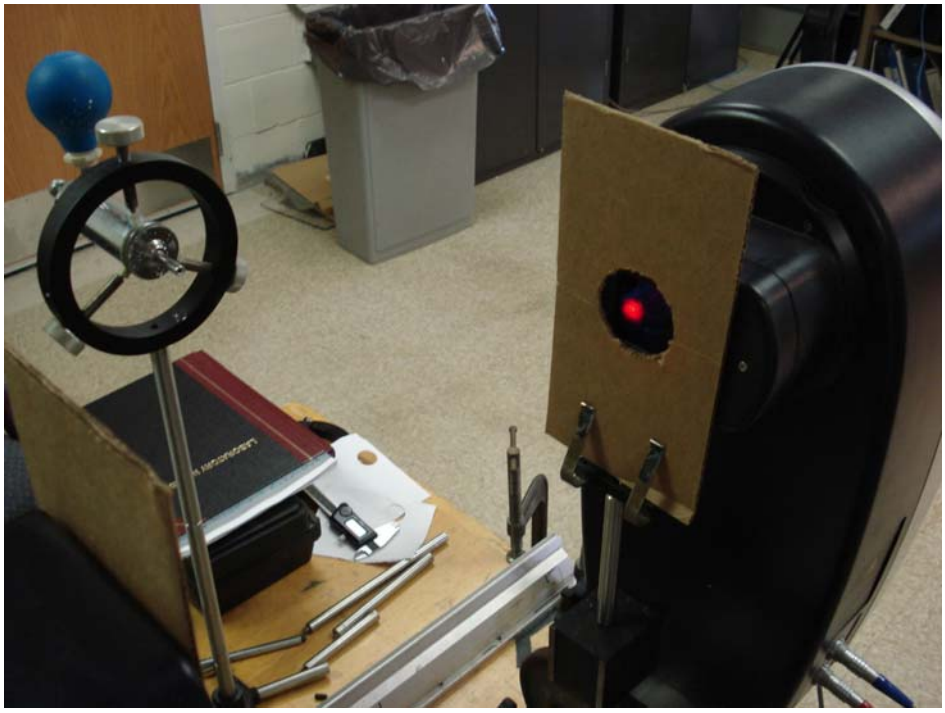

Fig. 2.35 – Experimental setup for testing the Malvern instrument through a hole

An air bulb puffer gun filled with zinc stearate, $\rho = 2.8$ g/cc, was used to conduct these small scale experiments. A control particle distribution was first obtained by measuring the particle distribution without any sort of hole interference 25 times. A 1" circular hole and a 2" circular hole were cut into pieces of cardboard and 25 more tests were then run to determine what effect, if any, testing through the hole had on the particle distribution (Fig. 2.36.)

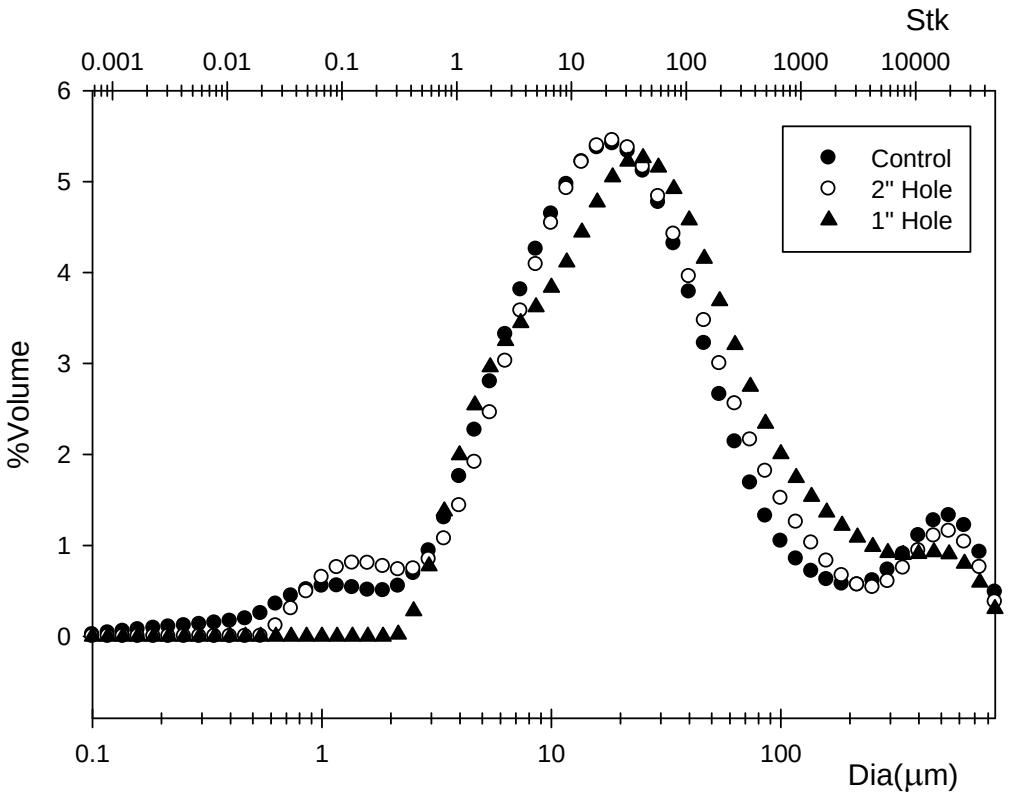

Fig. 2.36 – Particle distributions for control and two hole sizes

It is clear from this plot that at least a 2" hole is necessary to maintain an accurate measurement of particle distribution. The 1" hole has almost no reading below Stk~0.2, a shifted peak diameter, and a higher volume reading at Stk>~50. The 2" hole yielded the same peak and only slight variation in the range below Stk~0.3 and above Stk~100. Since the impactor is designed to remove any particles greater than Stk~1, the variation at the greater particle sizes is negligible as those particles should all be collected. Additionally, the discrepancy below the cutoff is not significant as those particles cannot reliably be impacted by this impactor. Therefore, as long as the hole used in the actual experiment is at least 2" in diameter, there will be no significant adverse effects to the measurement of particle distribution.

2.5.3 – Malvern Test: Inverted Through Glass

The next step was to make sure that the Malvern instrument could sample through the glass windows while inverted behind the impactor. 3" diameter holes were punched in each side of the ducting and covered with optical glass slides set in 'window frames' of

air-tight putty. It was necessary to ensure that the glass slides were perpendicular to the optical axis so that there was no diffraction by the windows that would skew the results seen in the bench-top test. The Malvern instrument has a function that allows the user to activate just the laser for alignment purposes. This feature, combined with the use of a level, was used to ensure the window positions. Because the frames were made from a putty, it was fairly easy to make adjustments to their positions. The window position was finally set when there was no visible reflection or refraction of the laser.

Once the setup was positioned, 25 tests with the bulb puffer gun were run and the distribution established. This was compared to the same control case that was used in the hole tests to determine what effect the glass and inverted orientation has on the measurement of the particle size distribution (Fig. 2.37.)

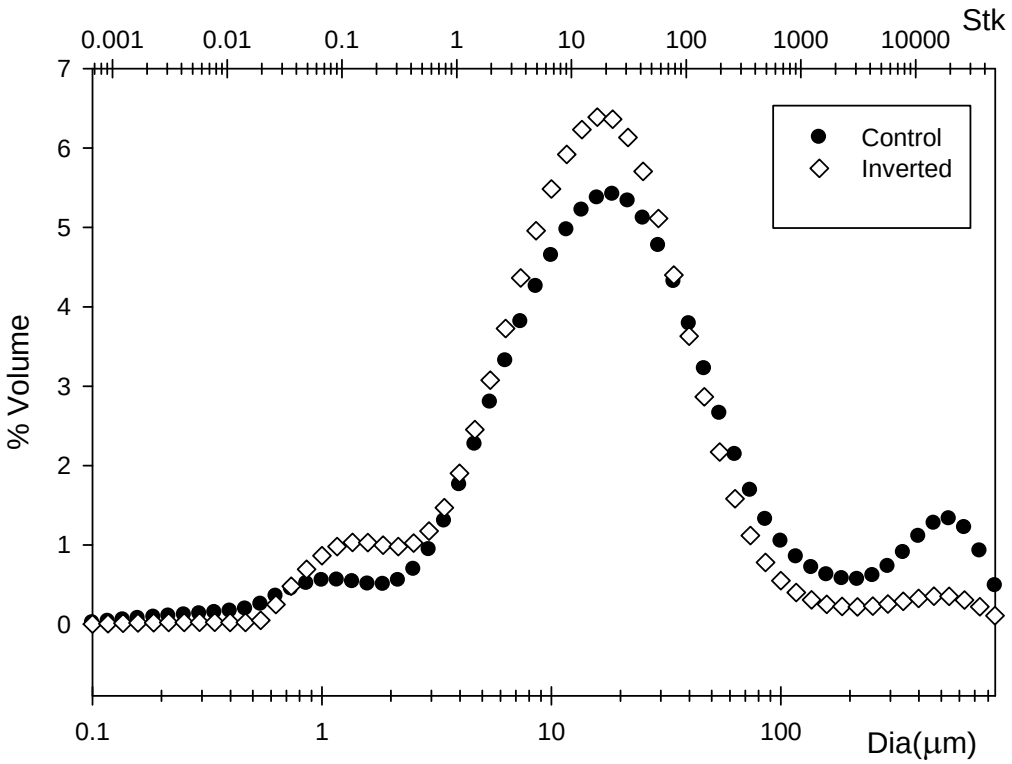

Fig. 2.37 – Comparison plot of inverted, glass test to control test

This plot shows that there is no detrimental effect to the measurement of either the glass or the inversion of the apparatus. The peak size is at nearly the same aerodynamic diameter, varying along the vertical axis only, and the variations high above the cutoff and far below can both be neglected as they lie outside the design space of this impactor.

Furthermore, since the distributions being compared will both be measured using this setup, the error will be consistent between them.

It has been clearly demonstrated that the experimental setup, testing through a glass-covered hole with the Malvern device upside-down from its standard operating position, does not introduce any additional appreciable error. The slight variations in particle size distribution measurement are in non-critical regions that are far enough away from the cutoff diameter that they should not affect the demonstration of impactor performance.

2.5.4 – Malvern Test: Comparison of Measured Talc Distribution to Standard

The same fluidizing bed setup used previously in the particle collection experiments was also the source of the particles for the full-scale particle distribution experiments done here. Before any comparative measurements could be made, it was necessary to confirm that the Malvern was yielding accurate results. The Penn State Materials Research Laboratory, MRL, was employed to size the talc being used for this experiment. This distribution was compared to the control case, impactor plates removed, to determine the level of measurement accuracy (Fig. 2.38.)

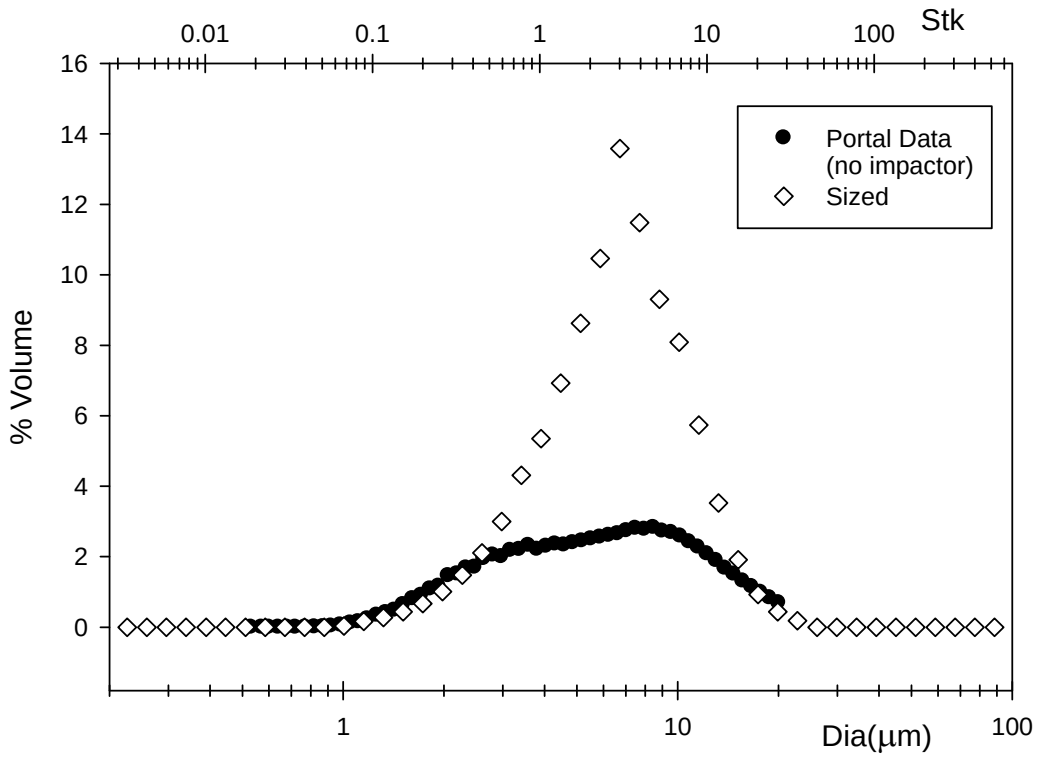

Fig. 2.38 – Comparison plot of MRL sized talc and fluidized bed talc

The distribution generated by the fluidized bed is roughly similar to that of the MRL-sized talc. While they are not exactly identical, the peaks occur at approximately the same particle size, ~8 μm from the fluidized bed and ~7 μm from the sized data, and the ranges of particle size are roughly equivalent. There are no particles generated by the fluidized bed that are significantly larger or smaller than what would be expected based upon the professional MRL sizing. Thus, the fluidizing bed could be relied upon to produce an accurate aerosolized flow of talc particles for the subsequent tests.

2.5.5 – Malvern Test: Impactor Particle Removal Comparison

The last step was to conduct tests run with the impactor plates in place. 25 test runs were measured, with the impactors being cleaned with acetone between each test to ensure that the incoming particle flow encountered the same impactor conditions. The results from this experiment were plotted along with the non-impacted case to gauge what shift, if any, is caused by the introduction of the impactor plates (Fig. 2.39)

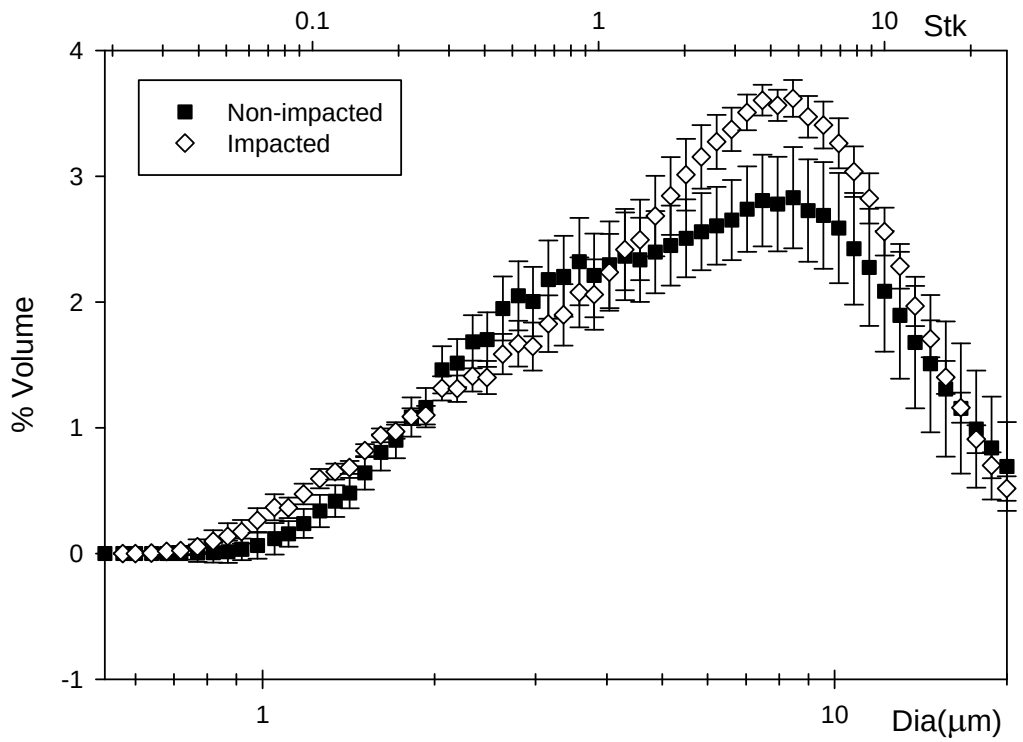

Fig. 2.39 – Comparison of particle distribution between non-impacted control case and impacted case

There is a notable change in the particle distribution between the two cases. The variation below the cutoff is slight, within the experimental error of one standard deviation. Above the cutoff diameter there is a significant change in the particle distribution. These data were used to generate an impactor efficiency curve using a ratio of collected particles, the difference between the two distributions in Fig. 2.39, to introduced particles, the control case. This efficiency curve created was clearly in error due to the magnitude of the removal being much too great and having a significant negative portion of the efficiency curve. Additionally, the position of the cut was determined to be around Stk~0.05, two orders of magnitude smaller than the design point and what was seen in the computational analysis of the impactor.

It was decided that the arbitrary nature of the dependent variable made it impractical to compare these two distributions to one another directly. Rather, the distributions must first be converted to a quantitative and concrete terms. The data produced by the Malvern sizer were presented as percent volume as a function of particle size. Using this, along with the assumption of volume introduced into the impactor from the Bernoulli analysis conducted for the microscope experiments, allowed for a simple

conversion to a particle count. Each distribution was normalized to the maximum diameter measured in each case (Fig. 2.40.)

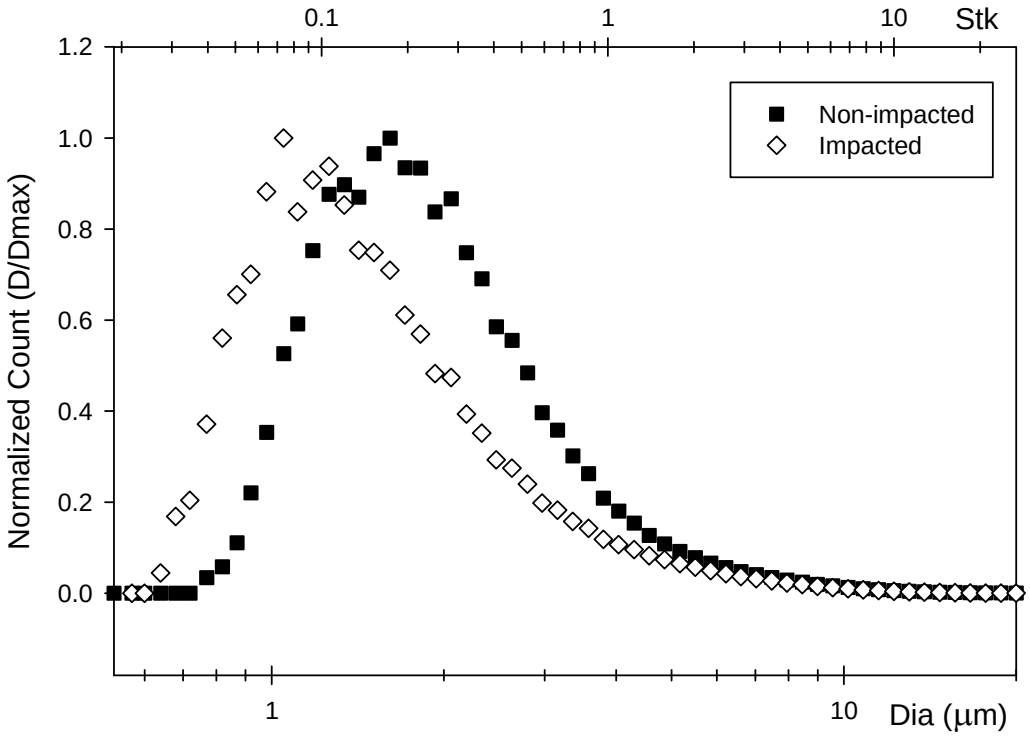

Fig. 2.40 – Malvern particle distribution data presented as particle counts

This conversion shows the change induced by the impactors in another, different way. The plot shows that the impacted case measures significantly more particles in the smaller size range as these are not removed from the flow. Assuming all other things equal, a larger portion of the total measured volume would be measured in this smaller size range due to the fact that the larger particles are removed. .

The impactor was designed to remove particles greater than Stk~1. Anything smaller than this target particle size cannot be reliably collected for interrogation. Therefore, it was assumed that the distributions would have to measure the same quantities of the smallest particles sizes regardless of whether or not the impactor plates were in position. To reflect this in the experimental results, each of the particle distritbutions was normalized to their respective values at this smallest point (Fig. 2.41.)

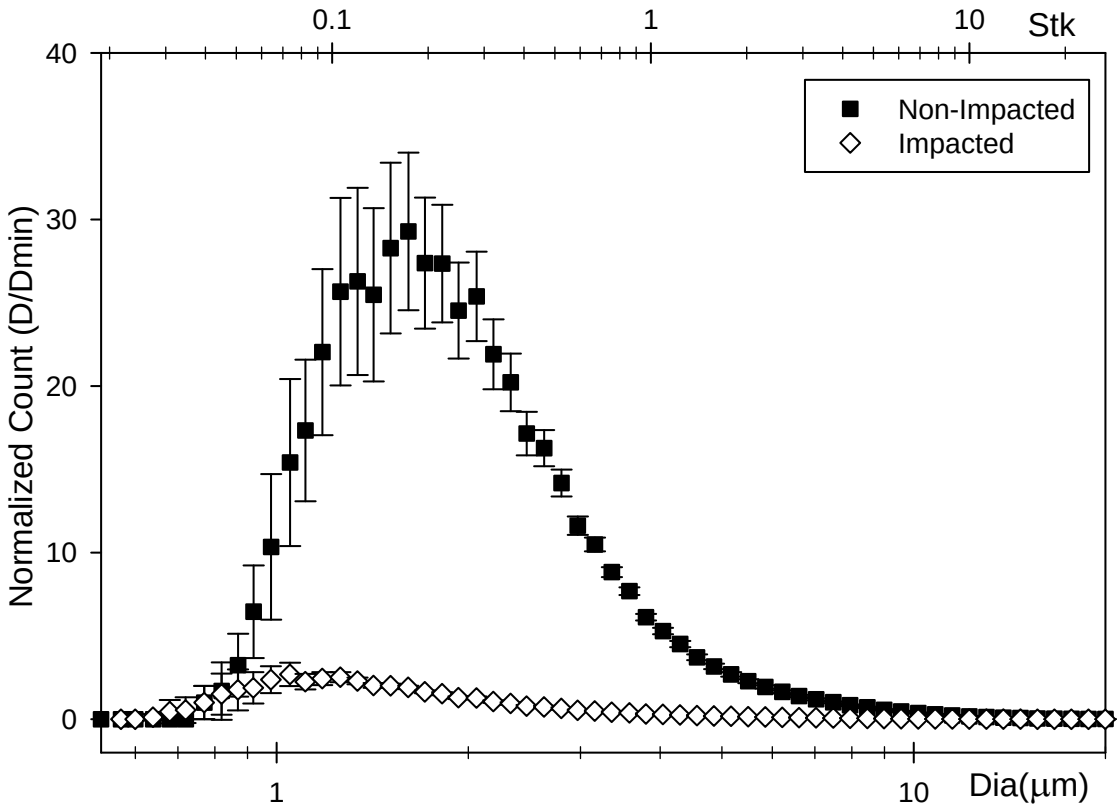

Fig. 2.41 – Particle counts normalized by smallest recorded diameters

Fig. 2.41 very clearly shows what is happening with the particle distribution. In the impacted case, once the particle size reaches Stk~1, the normalized counts are approximately zero. This change in distribution is indicitave of the impactor removing the larger particles from the bulk flow at the target diameter. Conversely, there is still a significant and measureable number of particles up until Stk ~10 in the open flow case. This is what would be expected to be seen as the maximum particle size in an unimpacted flow based up the maximum sizes reported by the professional sizing conducted by MRL (Fig. 2.38.)

Given the nature of the original source data, it was ultimately concluded that it would be impossible to generate a "typical" efficiency curve. However, the results of this experiment clearly show that there is a measurable change in the overall particle distribution. This change occurs in the upper ranges of particle size, where particle removal was intended, indicating that the impactors are removing the target particles from the bulk airflow.

2.6 – Conclusions on Impactor Efficiency Study

For any practical application of a particle impactor, an understanding of the impactor's efficiency is an important metric for overall system performance. Since the impactor for the wake sampling portal is so much larger than those previously studied, traditional methods were unable to be employed. Three methods were used to gain different points of comparison and to establish the effectiveness of the impactor.

Mircoscope slides were used to measure the distribution and impact locations of the collected particles. This experiment showed that particles of all sizes are collected by the impactor. It also determined that there is a significant concentration of particles towards the vertical and lateral center of the impact plates themselves, providing a location for additional improvements to be made in desorption methods scuh as grooving or the addition of a substrate. The locations of particle collection for a given particle size also provided insight into the cut diameter of the impactor. Once the particle size reached Stk~1, the distance away from center where particles of those larger sizes impacted narrowed considerably. This showed that a fundamental change had occurred in the flow behavior and, based upon the result seen, that the cutoff diameter had been reached.

As a point of comparison, the same experiment was done with a computational model. Overall impactor efficiency and impact locations were measured from a steady, fully-resolved FLUENT solution of the flow through the impactor. By releasing known quantities of particles with specified diameter and density, it was possible to generate the theoretical efficiency curve. The efficiency curve possessed the typical S-shape and showed the 50% cutoff point to be Stk~1, per the design point. Additionally, the range of impact locations began to narrow at this same point, reflecting the results seen in the microscope experiments and confirming the cutoff particle size.

Finally, the change in size distribution of particles within the flow was measured using the Malvern SprayTec particle sizer. After confirming that the particle distribution seen in the benchtop tests was not affected by being conducted upside-down, through holes and optical glass, the distributions were compared between impacted and unimpacted cases. There was a noticable change in distribution shape that, when scaled to counts and normalized by the count at an unimpacted diameter, showed the particles above Stk~1 falling almost completely out of the flow when the impactors were in place.

While the efficiency curve was not able to be generated from these data, these tests clearly demonstrated the change in overall particle distribution in the larger particle size range for which it was designed.

These three tests combine to demonstrate the effectiveness of the wake sampling portal impactor. By independently looking at the collection empirically and computationally, along with analyzing the change in particle flow behavior, the impactor performance has been proven. The impactor reliably removes particles from the flow in the size ranges for which it was designed. These particles are then concentrated towards the center of the impactor, making the desorption and interrogation of samples more reliable as these steps can be focused in the regions of the impactor plates where particles are known to collect. While the impactor efficiency curve was not able to be generated, these experiment show conclusively that the impactor is performing to its design specifications.

3.0 – Jet Timing Optimization

The air puffer portion of the portal was designed and built based upon a number of idealized assumptions: average human proportions, average walking speed, and the ability of all subjects to achieve and maintain an average walking speed goal. Upon testing, it became apparent that these assumptions were not ideal for timing the jets appropriately. After testing a number of different schemes, an optimized jet timing method was implemented to improve the performance of the air puffer portion of the wake sampling portal.

3.1 – Preliminary Jet Timing Scheme

The preliminary timing setup is based upon the assumptions listed above. The average-size human subject, moving at the prescribed 1.34 m/s, enters the portal, breaking the laser beam at the inlet and firing the front jets (Fig. 3.1.)

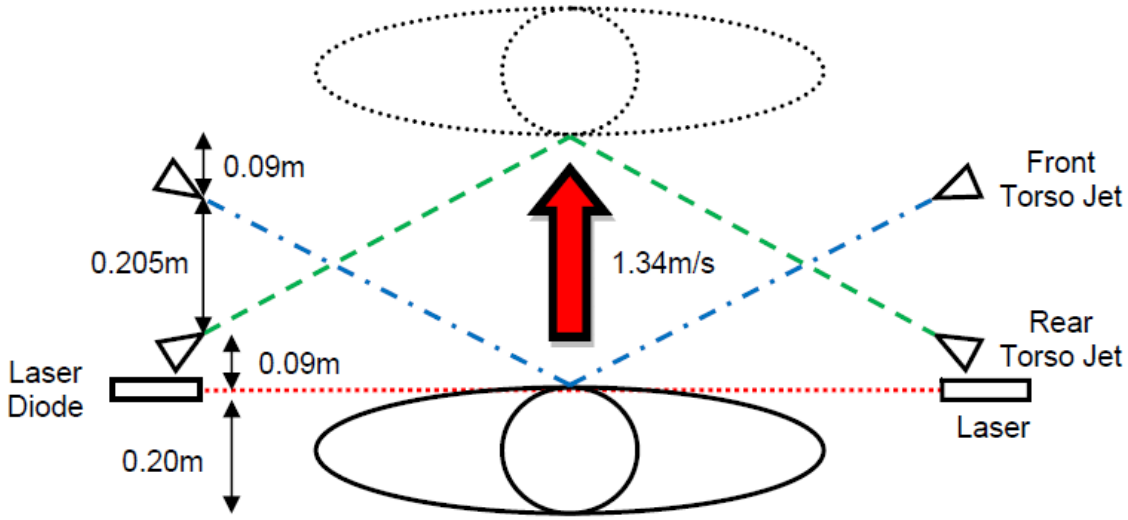

Fig. 3.1 – Initial air puffer jet triggering and timing scheme. Image from Volpe (7).

As the subject moves through the portal, the rear jets delay in firing for a short time, defined based upon the combination of the average thickness of a human subject, the distance needed to travel, and the assumed walking speed (Eqn. 3.1)

$$Delay = \frac{AverageSubjectThickness + PortalDepth}{WalkingSpeed} \qquad \text{Eqn. 3.1}$$

There are inherent shortcomings of this timing scheme due to the assumptions made. The general population varies in body size and type and there is no way to ensure that the subject will move at the 1.34 m/s design walking speed. These effects were observed directly by test subjects, who claimed that the rear jets were consistently hitting them in the sides, not on the back of the torso as desired.

3.2 – Optimized Jet Timing Scheme

Several different solutions were attempted to resolve the rear jet timing issue. Initially, the delay-timing algorithm was retained and devices to measure subject speed and depth as each different subject went through the portal were implemented. The level of complexity was reduced so as to incorporate two triggers, one for the front jets and one for the rear, but the timing of this method was still inaccurate.

The final design employed two triggers, however, it eliminated the need for measurements to be made or the need for a delay. The front jets triggered as the first beam was broken, similar to the initial design, however the aiming was adjusted to take into account the forward motion of the subject. Since the subject is progressing through the portal, the jets were focused slightly downstream of the front trigger to ensure the the subject was impacted in the desired locations. The rear jets were triggered by the second laser beam becoming unobstructed, that is, the subject breaks the beam and, when the photodiode "reconnects" with the laser, the rear jets fire (Fig. 3.2.)

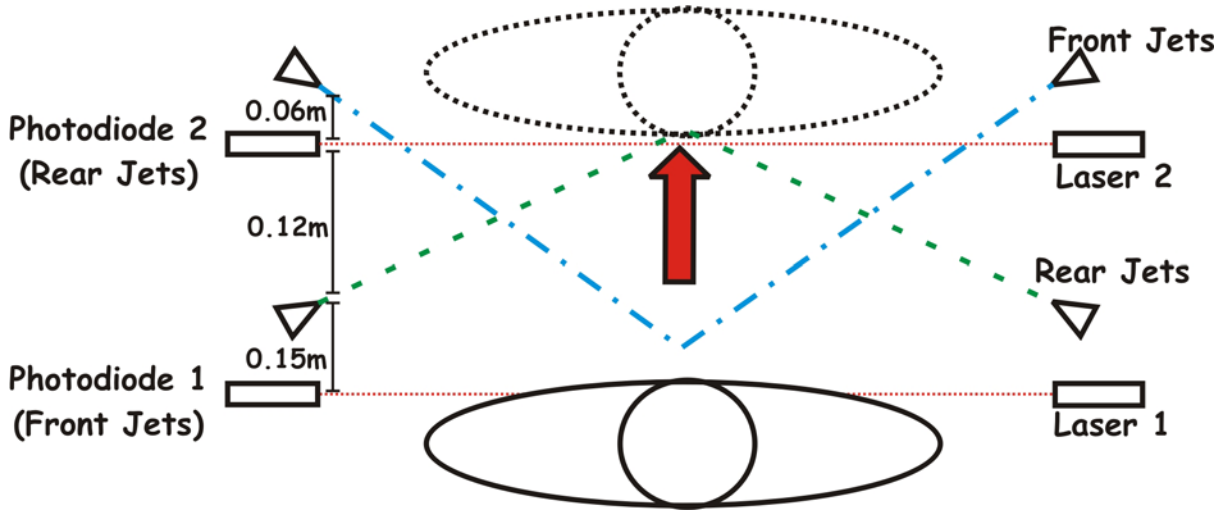

Fig. 3.2 – Optimized air puffer jet triggering and timing scheme

This timing scheme allowed a human subject of any size, moving at any 'brisk walking speed' to trigger the jets based upon their particular "run" through the portal. By eliminating any subject measurement or base-level assumptions from the determination of jet timing, the air puffer portion of the wake-sampling portal was optimized.

3.3 – Validation Experiment for Jet Timing

Since the claim by a human subject that the jets 'hit them on the back' is a highly subjective and qualitative scale to use in the demonstration of jet impact, a more quantifiable experiment had to be devised. 2" lengths of lightweight white string were sewn into a black shirt in a 1"-by-1" grid pattern (Fig. 3.3.). These acted as flow visualization "tufts".

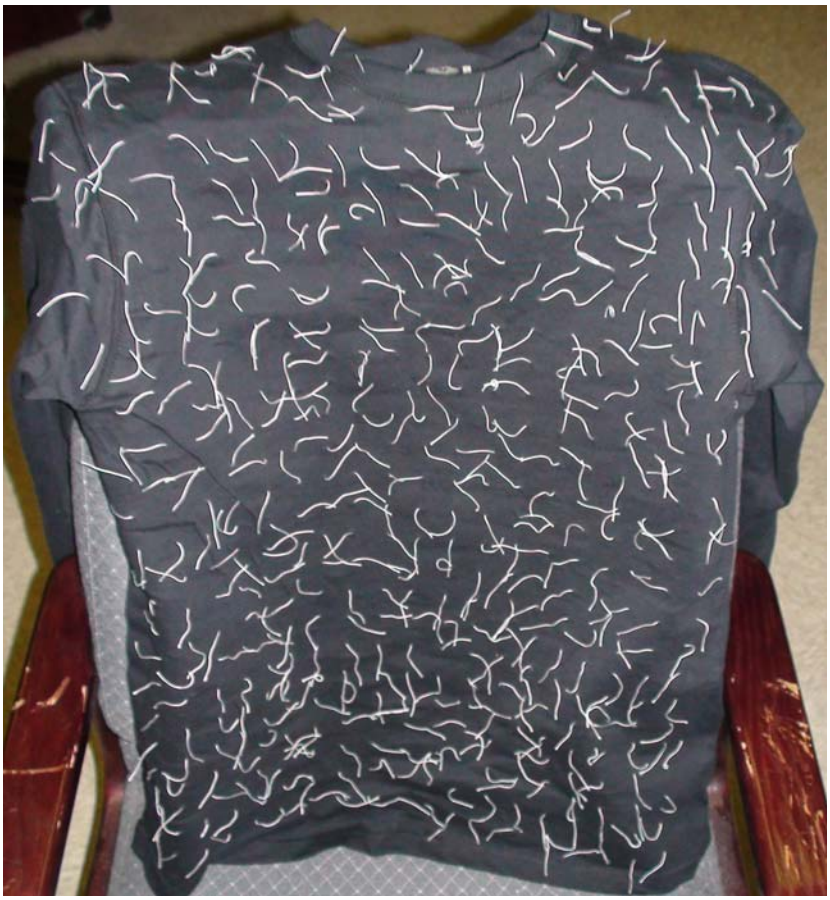

Fig. 3.3 – Tufted shirt for jet impact flow visualization

This shirt was worn by a human subject of average size and used to show the impact of jets on the torso. The goal was to have total coverage of the torso of the subject. This

would ensure that there were no torso surfaces that would go undisturbed for interrogation. Images were extracted from a high speed video immediately before and at the moment of jet impact to highlight the regions of the torso that were hit by the jets. Tests were conducted to adjust the aiming of the jets to ensure coverage from shoulders to waist and to ensure that the newly-implemented timing scheme was effective (Figs. 3.4-3.5.)

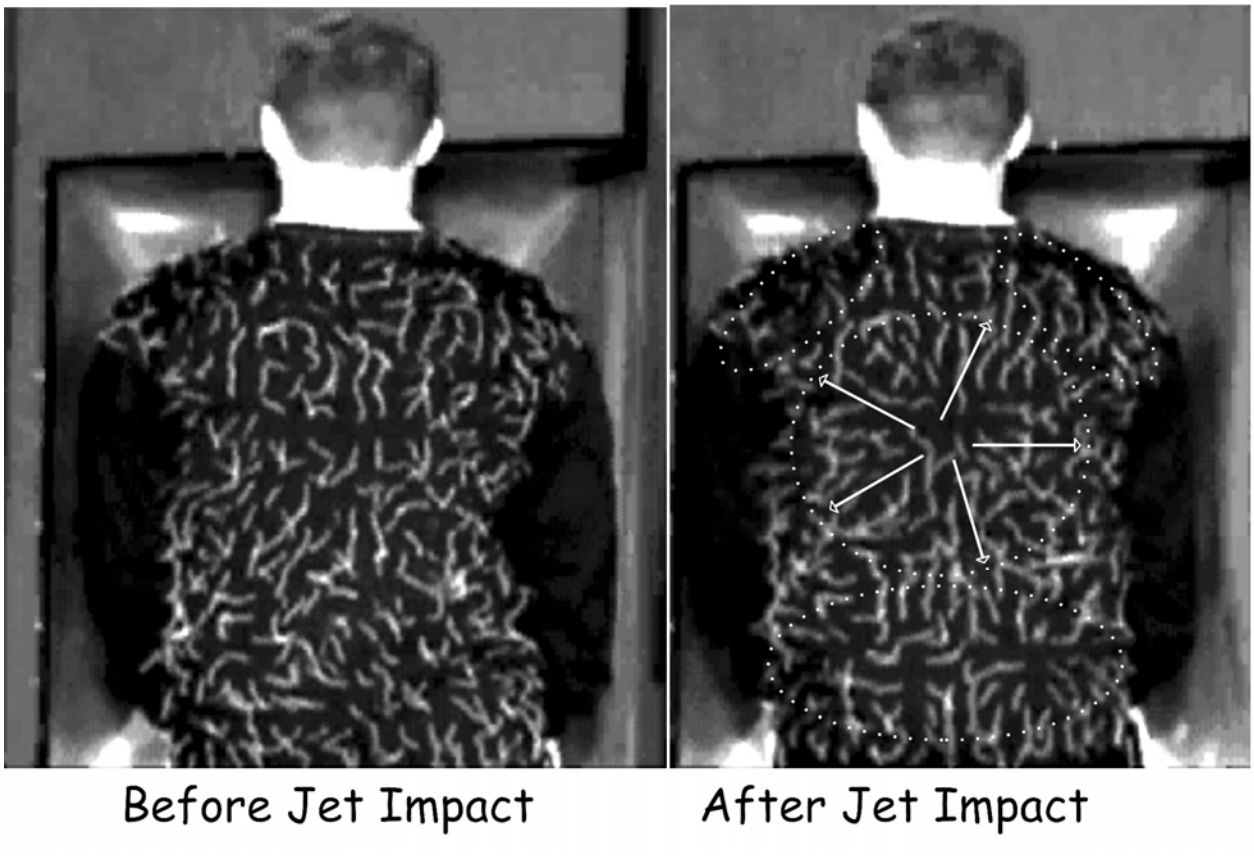

Fig. 3.4 – Tuft visualization of jet impact on the back of a human subject

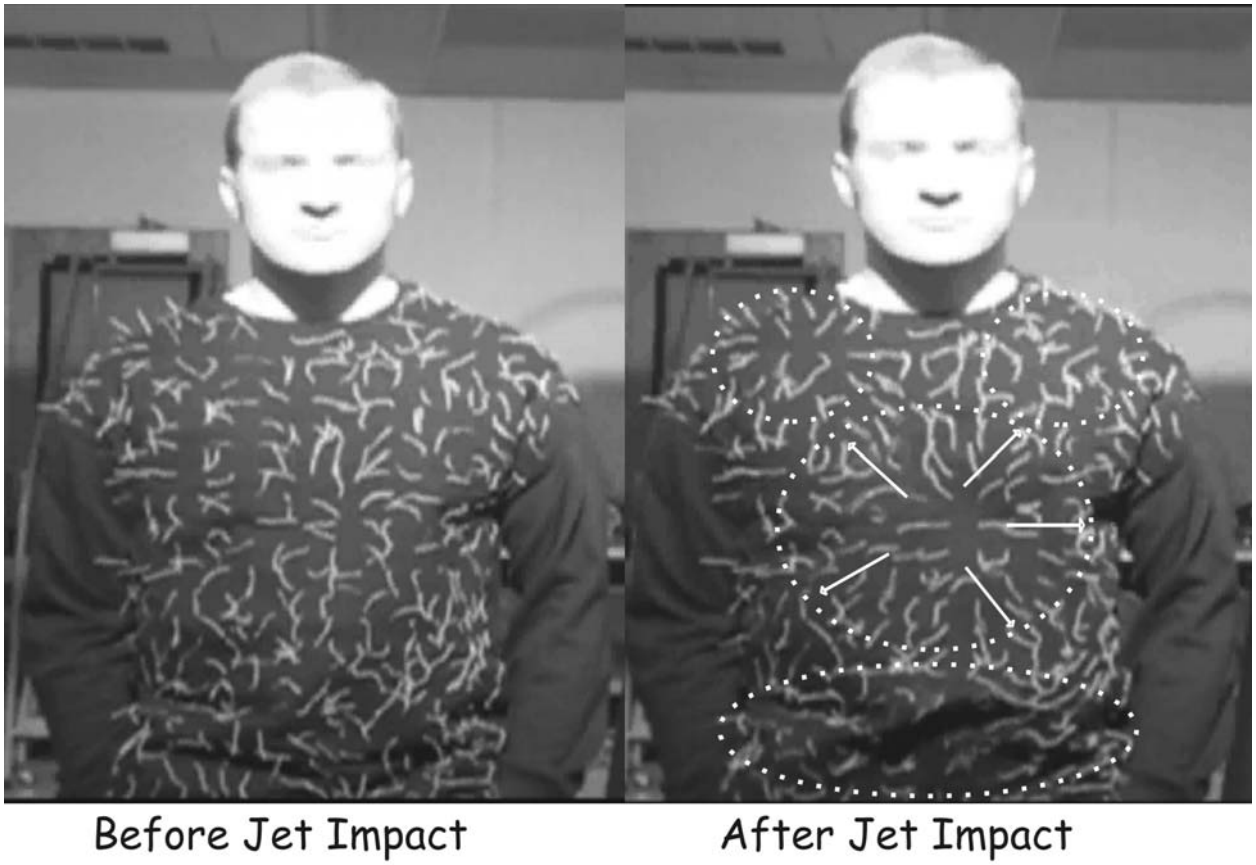

Fig. 3.5 – Tuft visualization of jet impact on the front of a human subject

The regions highlighted with white dotted circles and arrows are where the jets hit the subject, evidenced by the change in orientation of the tufts. It is clear that nearly the entire torso is impacted by the jets, thereby presumably dislodging particles from the majority of the subject's surface area.

These images therefore show that the current timing scheme is effective at impacting both the front and rear of the subject consistently and completely. Tests were run at walking speeds between 1.0 and 3.0 m/s to confirm that the variability in subject speed did not adversely affect the impact of the jets on the torso. Additionally, several subjects of different heights and body types were tested in the air puffer and it was found that jets were successful at impacting both sides of the subject. These experiments confirm that the timing and aiming of the jets in the air puffer section of the wake sampling portal have been optimized.

Chapter 4.0 – Wake Transport and Separation

The physical concept forming the foundation of this portal design is that of contaminated wake transport and separation. The concept was proven possible by Edge and Craven (4) (1). However, it was necessary to validate the effectiveness of this concept as implemented in the fully constructed breadboard portal. Laser sheet flow visualization was used to illuminate the fog-seeded wake of a human subject being transported and separated.

4.1 – Vertical Laser Sheet

The vertical laser plane was set at the center of the contraction to illuminate the wake behavior. A "stilling chamber", used to eliminate any momentum generated by the release of the jet of fog, was set up ~2 m from the entrance to the air puffer apparatus. The subject stood in the stilling chamber for ~10 seconds to allow the human thermal plume to develop and entrain the fog particles. Then the subject walked through the portal, transporting and separating the fog-seeded wake. Videos were taken perpendicular to the contraction inlet. This angle was chosen to highlight the transport, separation, and collection of the wake. The human subject enters the frame from the right and exits to the left. The wake can be seen as the illuminated region behind the subject. It is initially attached to the human, but separates and is directed into the aerodynamic contraction. Image sequences were extracted from the video, showing that the anticipated wake behavior is present in the portal (Fig. 4.1)

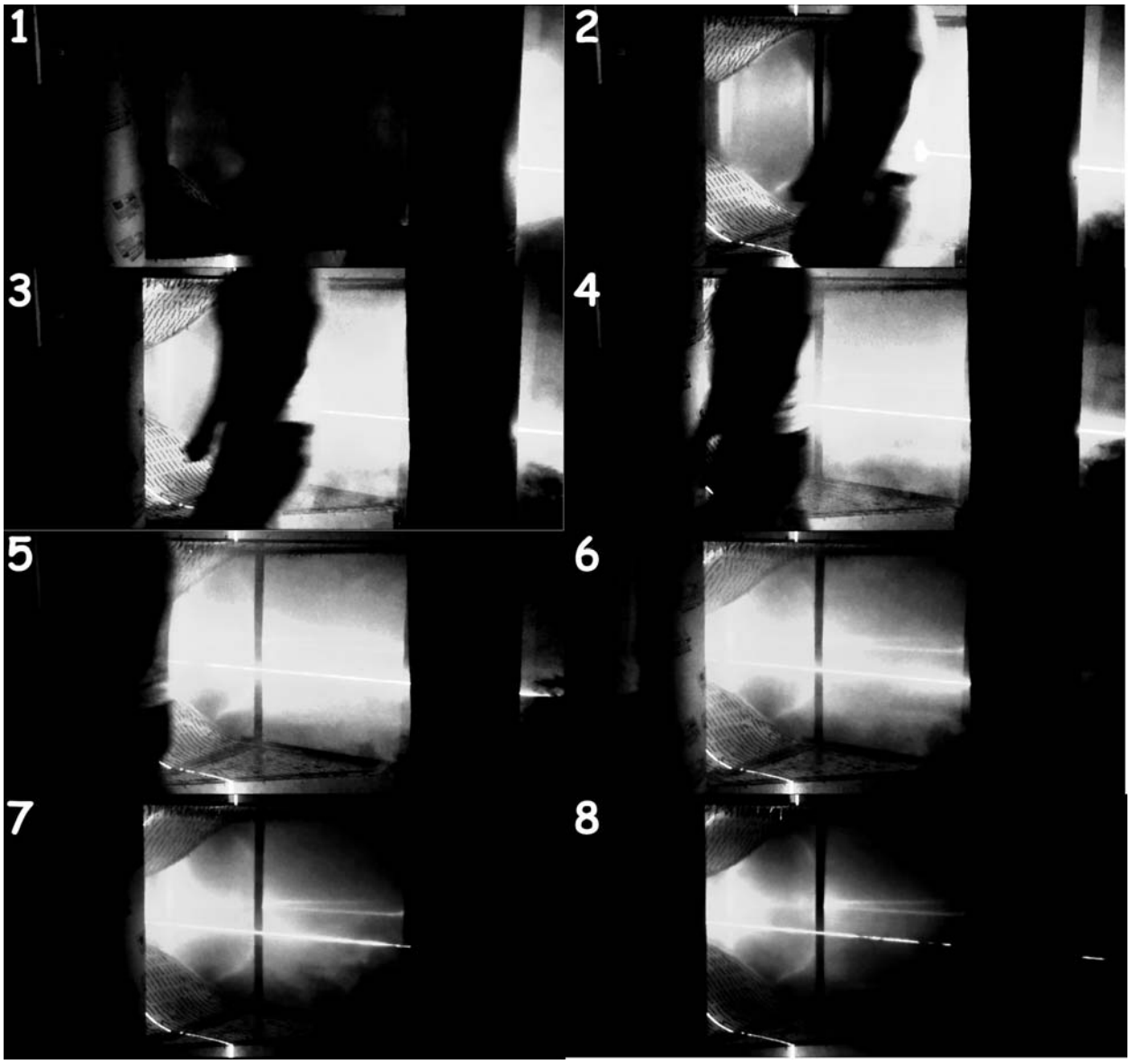

Fig. 4.1 – Images from vertical laser sheet showing transport and collection of fog-seeded wake.

The lighter portion of each of the above images is the wake making its progress through the portal and into the aerodynamic contraction. It starts attached to the human subject (frames 1, 2, and 3), but separates and proceeds downstream into the contraction and impactor (frames 4-8). This is indicative of the wake separation and collection phenomena upon which the portal designed was based. The wake is transported the ~2 m distance from the stilling chamber to the portal entrance, then the additional ~2 m through the portal itself before being separated and collected.

4.2 – Horizontal Laser Sheet

For comparison, the laser sheet was next rotated 90^{o} to be parallel with the floor. This second orientation was used to confirm the conclusion of successful wake transport and separation. The same experimental procedure used for the vertical laser sheet was employed in this case as well. The camera was placed above the contraction inlet, aimed down and slightly upstream, as seen in Fig. 4.2.

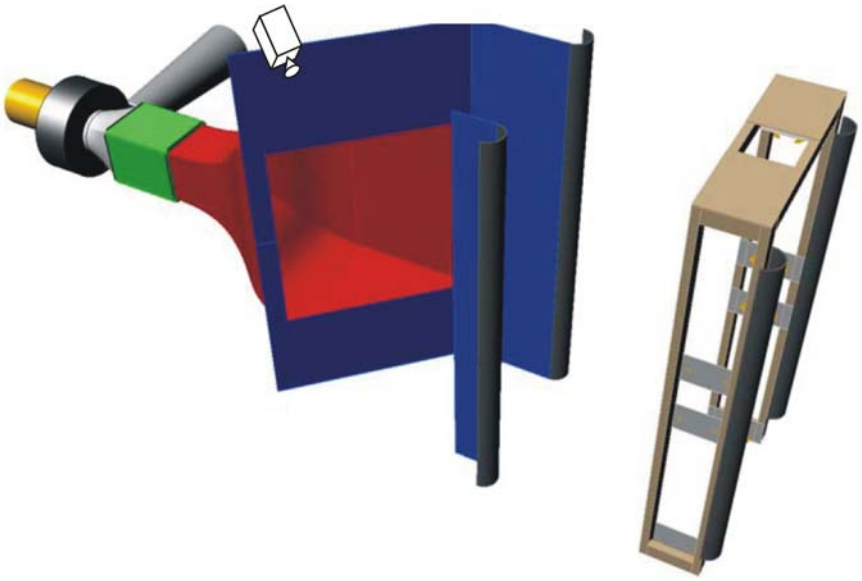

Fig. 4.2 – Camera location for horizontal laser sheet flow visualization

The video taken from this angle shows the human subject entering from the top center of the frame and exiting the bottom right corner. The illuminated wake is transported along with the human subject until the sharp turn, at which point the wake exits the bottom left corner of the frame and is collected into the aerodynamic contraction. A characteristic image sequence was extracted from the video to highlight wake flow (Fig. 4.3.)

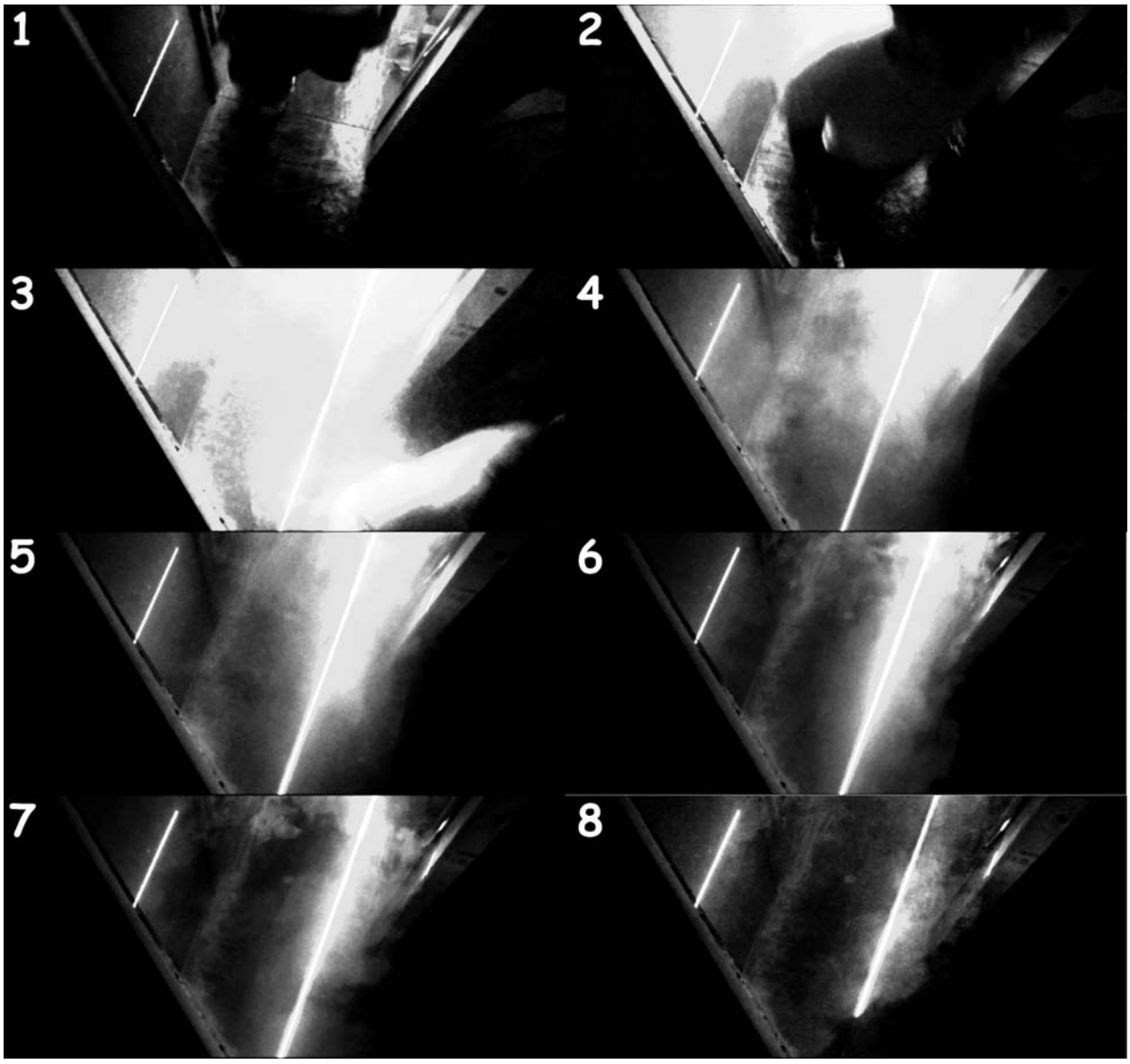

Fig. 4.3 - Images from horizontal laser sheet showing transport and collection of fog-seeded wake.

This orientation shows the wake behavior from above. The wake is seen as the bright region behind the human subject. It enters the portal and stays with the subject, separating in frame 2. Frames 3-8 show the wake being swallowed by the aerodynamic contraction and transported to the impactor for interrogation, similar to the behavior seen in the vertical laser sheet experiments, as well as in the work of Craven and Edge (1) (4).

These experiments show that the desired wake characteristics are maintained when implemented in the full wake sampling portal. The contaminated wake is transported through the portal to the aerodynamic contraction, where it separates from its

human subject and is collected by the inlet orifice and conveyed to the impactor. By conducting experiments similar to those done by Edge and Craven, it was possible to verify their results for this portal geometry and confirm that the aerodynamic wake sampling portal is operating to their specifications.

5.0 – Summary and Conclusions

5.1 – Project Summary

Increasing the throughput of airport security checkpoints is a worthy goal. Current trace portal technology required 10-30 seconds per subject, making it difficult to sample all passengers. Volpe (5) designed a portal to sample the trace signal trapped in the wake of a moving human subject based upon the work completed by Craven and Edge (1) (4). His design took many of the technologies used in current portals back to first principles and generated new geometries to optimize the effectiveness of each portal component in this new portal technology. These components then needed to be validated in "breadboard" portal experiments.

The most in-depth engineering study was done on the high-flowrate impactor. Volpe optimized the pressure drop, physical size, flow conditioning, and cutoff diameter design using computational fluid dynamics. By tracing streamlines through a fundamental model impactor, an optimized geometry was found that achieved all of the target goals. Following the construction, it was necessary to validate the real-world performance of the impactor at collecting trace signal from an aerosolized flow. Given the scale of this impactor, development of new empirical validation approaches was necessary.

Three different experiments were used to demonstrate the efficiency of the impactor. The computational model used in verifying the fluid flow in the final design of the impactor was expanded to include particle traces. These traces were used to generate a collection efficiency curve based upon particle size, which yielded the appropriate curve shape and target cutoff diameter. They also indicated the range of collection locations across the impactor face for those different particle sizes. As the particle size increased to the cutoff diameter and passed it, the range across the horizontal axis of the impactor where the particles impacted narrowed considerably. This second result was compared to results from microscopy experiments also being used to analyze the actual collection characteristics.

Microscopy was used to measure the variation in particle distribution along the vertical axis of each impactor face, the range of impact locations for particles of different size, and variation in collected particle concentration distribution between the three

impactor plates. This first experiment verified that there was no variation in vertical collection location based upon particle size. There was a roughly-normal distribution from top to bottom, with a slight increase in particle concentration at the center of the vertical axis, as would be expected for a flow of this nature. This conclusion allowed the remainder of the experiments to be focused on the vertical center of the impactor without any loss in data fidelity.

The second experiment provided a point of comparison for the results of the CFD deposition analysis. The range of particle impacts did not directly correlate between the two studies; however, the trends seen were similar in both cases. Both studies showed particles below the cutoff diameter being impacted all over the impactor face. Once the particle size reached the target cutoff diameter, the range narrowed to a much-more-concentrated band centered at the centerline of the impactor face. This shows that the larger particles are being removed from the bulk airflow and being collected towards the center of the impactor, an important point to know for the future refinement of the impactor face.

The final experiment showed that there was a slight flow bias away from the left-hand side of the aerodynamic contraction and the impactor. The number of particles collected on the center and right-hand impactors was almost identical, while the number collected on the left-hand impactor was somewhat less. Hot-wire anemometer, laser sheet, and tuft flow visualization were used to verify that there was a flow bias away from the leftside. The hot-wire test revealed that there was a much lower velocity at the impactor inlet on the left-hand side. The flow visualization techniques revealed that this was due to a large recirculation region on that side at the aerodynamic contraction inlet. Fairings were installed to condition the flow and the flow bias was reduced at the impactor.

The jet timing algorithm was rewritten to eliminate assumptions based upon average human size and an average, constant walking speed in favor of independent triggers for the front and rear jets. A tufted shirt was worn by a human test subject to validate the timing scheme and the aiming locations of the jets. The experiment showed that the new triggering method reduced the error introduced due to the human factors.

This new timing method allowed the air-jets to consistently and completely agitate the front and the rear of subjects of varying size moving through the portal at various speeds.

The final experiment validated the wake separation aspect of the portal design. Laser sheet flow visualization was used to show that the human wake, seeded with theatrical fog, could be transported from the portal entrance, through the jet puffer apparatus, separated at the 45^{o} turn, and collected into aerodynamic contraction inlet. The possibility of this concept had been confirmed by Craven (1), however it was necessary to show that it was being effectively implemented in the breadboard aerodynamic wake sampling portal. Vertical and horizontal laser sheet flow visualization confirmed that the wake is transported into the portal, separated by the sharp turn, and collected into the aerodynamic contraction for collection and interrogation. From this experiment, the fundamental physical concept driving the design and implementation of the breadboard portal was verified.

5.2 – Future Work

The preliminary performance evaluation has been completed. The breadboard portal has been shown to successfully perform its three primary tasks to the specifications of the portal design and per the conceptual guidelines. This section serves to outline future areas of interest that the Penn State Gas Dynamics Lab plans to investigate.

Further optimization of the air puffer portion of the portal

There is presently adequate coverage of the torso of a human subject of average size. The addition of more jets would serve to agitate and interrogate more completely any human subject entering the portal. These jets could be dynamically implemented with an array of lasers and photodiodes measuring the subject's height as they enter the portal and activating the jets that correspond to a subject of that height (Fig. 5.1.)

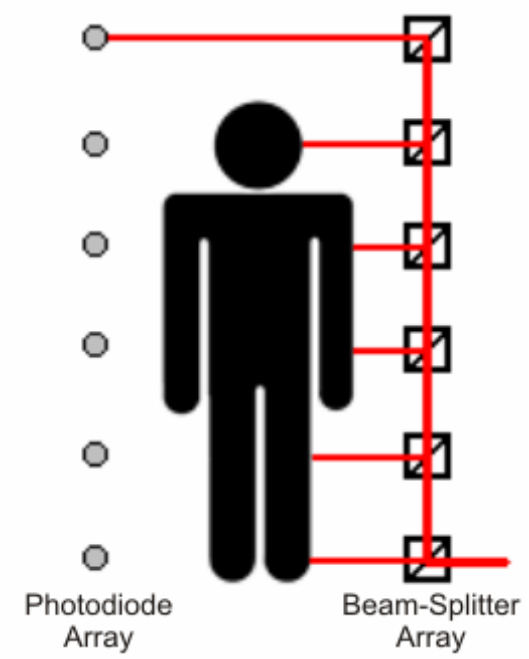

Fig. 5.1 – Height-measurement optical system for implementation to aerodynamic wake sampling portal

Flow visualization of trace removal from the human subject

It is well documented that impinging jets generate a shear stress upon their target surface, and that this shear stress is strong enough to remove particulate trace matter from the subject. However, the effectiveness of this technology in a portal of this type, one in which the human subject is moving and not stationary, has not been confirmed. It could be possible to seed the human subject with particles and then visualize and quantitatively measure the removal. This would be a valuable tool in the further optimization of the wake sampling portal.

Particle image velocimetry validation of flow visualization conclusions

Several conclusions regarding the flow behavior at various locations throughout the flow path of the portal were drawn based upon qualitative measurements from laser sheet and tuft flow visualization techniques. While believed accurate, these conclusions lack a quantifiable measurement that could be used to gauge the level of improvement achieved in the flow conditions. Measuring the velocity field through the contraction with and without the fairing would provide another check on the solutions implemented currently. PIV could also be used to further explain and help eliminate any rightward flow bias that

the entering flow may have. It could also be used to explain the true nature of the particulate matter recirculating in the human wake, how well it gets entrained and separated, and where portal flow conditions may trap and isolate the trace signal and prevent it from being interrogated at the impactor.

Acoustic treatment

The breadboard portal may be too loud during operation. The blower generates a large amount of acoustic noise that needs to be addressed. Ducting the exhaust flow out of the room, combined with some damping, baffling, and other noise-control solutions, could be used to reduce the noise issue.

Impactor improvements

The impactor has been shown to remove trace particles from the bulk airflow and concentrate them on the impactor face for easy desorption and interrogation. However, there exist other methods to improve impactor performance, such as grooving the face or the application of a 'sticky' substrate. These methods could be implemented and have the potential to drive the cutoff diameter down even lower, allowing the collection and interrogation of a larger portion of the trace signal available in the human aerodynamic wake, even to the point of sampling vapor. Additionally, the development of a method to sample the collected trace and clean the impactor plate internal to the impactor itself would greatly aid in the reduction of analysis time. The lower limit in throughput time has been reached based upon the aerodynamics of the system. The holdup now is the signal analysis portion of the portal. Improvements such as these could further reduce the time between subject interrogations.

Aerodynamic contraction improvements

The flow visualization experiments conducted on the contraction portion of the portal indicate that there exists the need for a redesign. There is a complex, dual-inflection-point wall profile curve currently in use on the left side of the contraction due to the necessary addition of the entrance fairing. A relaxation of this wall geometry could serve to further increase the level of flow uniformity at the impactor inlet plane. This could, in

turn, provide more consistent and dependable collection characteristics on the impactor itself.

Explosive simulant patch tests

Explosive patch testing serves as a full-system validation technique for portal performance. While each major phase of the portal has been independently validated, the patch tests present a real-world way to test the portal as a whole. The Penn State Gas Dynamics Lab has a method of conducting these patch tests. By incorporating a second, independently-generated patch test experiment, an important point of comparison in the overall portal performance would be obtained. These tests could be conducted following any major change in flow path or characteristics to determine the net positive or negative effect on the portal produced by these changes.

Construction "clean-up" of the breadboard portal

The ultimate goal of this design project is to develop a working, testable prototype portal to be subjected to the rigorous validation process of the TSL. To achieve this ultimate goal, it may be necessary to reconstruct or modify some of the existing components to meet the standards required for the portal to be tested in this manner.

References

1. Craven, B. A. and Settles, G. S.. The Design of a Chemical Trace Detection Portal that Samples the Aerodynamic Wake of a Walking Person. 2006.

2. Settles, G. S.. Chemical trace detection portal based on the natural airflow and heat transfer of the human body. [6,073,499]. 6-13-2000. US Patents.

3. Craven, B. A. and Settles, G. S., "A computational and experimental investigation of the human thermal plume," *Journal of Fluids Engineering*, Vol. 128, 2006, pp. 1251.

4. Edge, B. A., Paterson, E. G., and Settles, G. S., "Computational study of the wake and contaminant transport of a walking human," *Journal of Fluids Engineering*, Vol. 127, 2005, pp. 967.

5. Volpe, J. A.. The Design of an Aerodynamic Wake Sampling Portal. 2007. University Park, PA, Pennsylvania State University.
   Ref Type: Thesis/Dissertation

6. Marple, V. A., Rubow, K. L., and Olson, B. A., "Inertial, gravitational, centrifugal, and thermal collection techniques," *Aerosol Measurement: Principles, Techniques, and Applications*, 2001, pp. 229-260.

7. Chang, M., Kim, S., and Sioutas, C., "Experimental studies on particle impaction and bounce: effects of substrate design and material," *Atmospheric Environment*, Vol. 33, No. 15, 1999, pp. 2313-2322.

8. Marple, V. A. and Willeke, K., "Impactor design," *Atmospheric Environment (1967)*, Vol. 10, No. 10, 1976, pp. 891-896.

9. Verkouteren, J. R., "Particle Characteristics of Trace High Explosives: RDX and PETN," *Journal of Forensic Science*, Vol. 52, No. 2, 2007, pp. 335-340.

10. Annapragada, A. and Adjei, A., "An analysis of the Fraunhofer diffraction method for particle size distribution analysis and its application to aerosolized sprays," *International Journal of Pharmaceutics*, Vol. 127, No. 2, 1996, pp. 219-227.